Materials Advances

Accepted Manuscript

This article can be cited before page numbers have been issued, to do this please use: Z. Falah Khudair, F. A. Nelson, K. Etim, K. W. Qadir and M. Runde, *Mater. Adv.*, 2026, DOI: 10.1039/D6MA00432F.

ROYAL SOCIETY OF CHEMISTRY

rsc.li/materials-advances

View Article Online
DOI: 10.1039/D6MA00432F

Availability of data

The data supporting this study are available in the Supporting Information. Additional computational log files and raw data are available from the corresponding author upon reasonable request.

Structure-Property Relationships in Heteroatom-Doped g-C_3N_4 Nanocarriers for Cimetidine: A Computational Study

Zharaa F. Khudair, Favour N. Azogor[2]*, Kingsley Etim[3], Karwan W. Qadir[4], Runde Musa[5,6]

[1]*Department of Chemistry, College of Education, University of Al-Qadisiyah, Al-Diwaniyah, Iraq*

[2]*Department of Pure and Applied Chemistry, University of Calabar, Calabar, Cross River State*

[3]*Department of Chemistry, Modibbo Adama Federal University of Technology, Yola, Nigeria.*

[4]*Department of Physics, College of Education, Salahaddin University-Erbil, 44002, Erbil, Kurdistan Region, Iraq*

[5] *Department of Research Analytics, Saveetha Dental College and Hospitals, Saveetha Institute of Medical and Technical Sciences, Saveetha University, Chennai, India.*

[6] *National Open University of Nigeria (NOUN), Abuja, Nigeria*

*Corresponding Author: azogorfavour@gmail.com

Abstract

In this work, a comprehensive density functional theory (DFT) and Monte Carlo molecular dynamics (MD) investigation is conducted to evaluate the interaction of cimetidine (Cmt), an anti-ulcer drug, with pristine and X-doped C_3N_4 surfaces (X = B, S, P, and Si). Adsorption energy calculations reveal favorable and thermodynamically stable binding of cimetidine on pristine C_3N_4 as well as B-, S-, and Si-doped C_3N_4 surfaces, characterized by moderate physisorption energies suitable for reversible drug loading and release. Natural bond orbital (NBO) and density of states (DOS) analyses demonstrate pronounced charge transfer and orbital hybridization upon adsorption, particularly for doped systems, confirming the role of dopants in tuning surface reactivity. QTAIM and noncovalent interaction (NCI) analyses identify a combination of hydrogen bonding, electrostatic, and van der Waals interactions governing adsorption stability. Molecular dynamics analysis reveals that B@C_3N_4 exhibits pronounced time-dependent diffusion behavior, characterized by reduced cimetidine mobility at short simulation times (100 ps) and enhanced diffusion at longer times (500 ps), indicating effective initial drug retention followed by facilitated release. In contrast, Si@C_3N_4 exhibits more uniform diffusion behavior across both time scales, suggesting steady and controlled drug delivery. The results highlight doped C_3N_4 as a promising platform for controlled cimetidine

View Article Online
DOI: 10.1039/D6MA00432F

delivery, providing fundamental insights into the structure–property relationships governing drug–nanocarrier interactions.

Keywords: *Cimetidine; Drug Delivery; Monte Carlo; MD; DFT*

1.0 Introduction

The rapid decline in the prevalence of *Helicobacter pylori* infection, together with the widespread use of potent anti-secretory drugs, has resulted in a substantial reduction in peptic ulcer disease compared with two decades ago [1]. Following the 1994 NIH consensus conference, which recommended that all patients with peptic ulcers be tested and treated for *H. pylori*, numerous studies have confirmed that successful eradication therapy markedly lowers ulcer relapse rates. However, long-term outcome data remain relatively limited [2]. Significant developments that have contributed to the decreased incidence of peptic ulcer disease include the introduction of highly effective acid-suppressive agents, which have transformed the understanding of ulcer pathogenesis and management. Nevertheless, the disease remains clinically significant, mainly due to the increasing global use of non-steroidal anti-inflammatory drugs (NSAIDs) and low-dose aspirin, both of which are major contributors to ulcer formation and associated complications [3].

Several studies have conclusively demonstrated the effectiveness of sulfur doping as a strategy to tailor graphene for high-performance biosensing applications. Ren *et al.* showed that sulfur-doped graphene sheets, synthesized via click chemistry and used as the structural framework in a tri-antibody dual-channel immunosensor, significantly enhanced signal transduction and stability, enabling ultralow-level detection of cancer biomarkers such as CEA and NMP22 in clinical urine samples [4]. Li *et al.* further demonstrated that controlled sulfur doping, particularly in the form of homogeneous thiophenic sulfur, induces lattice distortion, curvature, and porous microstructures in graphene, resulting in markedly enhanced electrocatalytic activity and sensitivity in dopamine biosensing [5]. Importantly, Shahzad *et al*. reported that biomass-derived sulfur-doped reduced graphene oxide exhibits strong electron-donating characteristics and improved electrical conductivity, leading to robust sensitivity, wide linear detection ranges, and excellent selectivity for the cancer risk biomarker 8-hydroxy-2′-deoxyguanosine (8-OHdG) [6]. A growing body of literature demonstrates that other heteroatom dopants, including boron (B), phosphorus (P), and, to a lesser extent, silicon (Si),

View Article Online
DOI: 10.1039/D6MA00432F

can also effectively tailor graphene-based materials for biosensing, sensing, and biomedical applications. Boron-doped graphene has been shown to modulate charge distribution and introduce p-type character, leading to enhanced electron-transfer kinetics and improved electrochemical responses toward biologically relevant analytes, as demonstrated in enzymatic and NADH-related biosensing platforms by groups such as Lazar *et al*. and others [7], [8], [9]. Phosphorus-doped graphene, characterized by enlarged lattice distortion and electron-rich defect sites, has been widely reported to exhibit enhanced electrocatalytic activity and sensitivity in chemical and biological sensors, with several studies highlighting its suitability for electrochemical detection of biomolecules and pollutants [10]. In contrast, silicon-doped graphene has been less extensively explored experimentally in biosensing, with most reports focusing on theoretical predictions and electronic-structure modulation; nonetheless, these studies suggest that Si incorporation can significantly alter adsorption behavior and surface reactivity, indicating potential for future sensor development [11], [12]. In parallel, g-C_3N_4 has emerged as a versatile metal-free semiconductor for biosensing and biomedical applications owing to its tunable band structure, chemical stability, and abundant nitrogen-rich active sites. Numerous studies have reported pristine and doped g-C_3N_4 as effective platforms for electrochemical, photoelectrochemical, and fluorescent biosensors [13], [14]. Importantly, heteroatom doping of g-C_3N_4, particularly with boron or phosphorus, has been shown to further enhance charge separation, surface reactivity, and analyte adsorption, enabling ultrasensitive detection of biomolecules such as dopamine, metal ions, and viral or cancer-related biomarkers, as demonstrated by Demirici *et al*. and Li *et al* [15], [16] [17]. In parallel with advances in heteroatom-doped graphene and g-C_3N_4 platforms, there is a clear clinical demand for improved diagnostic and therapeutic strategies in gastrointestinal diseases. In the context of peptic ulcer therapy, Ford *et al.* conducted a comprehensive systematic review and economic analysis of 52 clinical trials, demonstrating that Helicobacter pylori eradication therapy yields superior healing outcomes compared with conventional acid suppression, with pooled healing rates of approximately 90% for duodenal ulcers and 85% for gastric ulcers, alongside a marked reduction in long-term recurrence [18]. Beyond therapy, gastrointestinal drugs such as cimetidine have also been explored for diagnostic applications; for example, Sanad *et al.* reported that radio labeled ^{125}I-cimetidine exhibits high and selective uptake in ulcerated gastric tissue, highlighting the feasibility of ulcer-targeted imaging approaches. Building on this concept of targeted delivery and localization, graphene-based nanomaterials have emerged as promising carriers for gastrointestinal drugs [19].

View Article Online
DOI: 10.1039/D6MA00432F

Despite the remarkable potential of graphene-based nanostructures in therapeutic applications, their performance can be significantly limited by weak drug–surface interactions, uncontrolled release behavior, and inadequate electronic sensitivity. To address these challenges, heteroatom doping has emerged as a powerful strategy for chemical tailoring, enabling precise modulation of surface reactivity, electronic structure, charge distribution, and binding affinity. Dopants such as boron (B), sulfur (S), phosphorus (P), and silicon (Si), originating from different groups in the periodic table (3, 6, 5, and 4, respectively), introduce distinct electronic perturbations that profoundly influence adsorption mechanisms. Their contrasting electronegativities, covalent radii, and valence-electron configurations alter the graphene framework in unique ways, resulting in tunable π systems, localized charge polarization, defect formation, and enhanced active sites for molecular anchoring. Heteroatom doping and surface functionalization have recently been proven to be effective strategies to improve the performance of carbon nitride-based materials in a variety of applications. For example, Khajavian et al. found that co-doping and metal decoration of C_2N nanosheets can greatly enhance the adsorption performance for pharmaceutical compounds, due to the generation of extra active sites and stronger surface interactions [20], [21]. In the same way, Kaviani et al demonstrated that functionalization of a C_3N_3 nanosheet using thiophene results in a significant improvement of electronic properties, such as a reduction in the band gap and better charge transport, which are essential to energy storage systems for the adsorption and diffusion of ions [22]. Moreover, adsorption energy and stability of carbon nitride frameworks can be considerably tuned by structural modification, further confirming the sensitivity of the system with respect to the surface chemistry, as indicated by related findings. These effects make X-doped graphene an attractive platform for regulating drug adsorption strength, stability, and controlled release, particularly for pharmaceutical molecules with multiple functional groups such as cimetidine, an anti-ulcer drug widely used in gastrointestinal therapy. Understanding how different dopants influence the physicochemical interactions between graphene and cimetidine is therefore critical for designing safer, more efficient, and stimuli-responsive drug-delivery systems.

2.0 Computational Details

All quantum-chemical calculations in this study were performed using density functional theory (DFT) to investigate the structural, electronic, and adsorption properties of pristine and X-doped graphene-like C_3N_4 sheets (X = B, S, P, Si) interacting with the cimetidine (Cmt) drug molecule. Geometry optimizations and energy evaluations were carried out using the PBE0

View Article Online
DOI: 10.1039/D6MA00432F

hybrid functional, which incorporates a balanced mixture of exact Hartree–Fock exchange and generalized gradient approximation exchange–correlation, providing improved accuracy for heterogeneous systems and noncovalent interactions [23]. To account for dispersion effects critical in physisorption and drug–surface interactions, Grimme's D3 empirical dispersion correction with Becke–Johnson damping (PBE0-D3) was applied throughout the calculations [24]. The Def2-SVP basis set was employed for all atoms during structural optimization, offering a reliable balance between computational efficiency and accuracy for medium-sized molecular systems [25]. Adsorption energies were computed to evaluate the affinity between cimetidine and the doped surfaces using the formula in equation **(1)** [26].

$$E_{ads} = E_{complex} - (E_{C_3N_4/X@C_3N_4} + E_{cmt}) \quad (1)$$

where E_{complex} is the total electronic energy of the adsorbed system, $E_{X@C_3N_4}$ is the energy of the pristine C_3N_4 surface and the doped surfaces $X@C_3N_4$, and E_{cmt} represents the energy of cimetidine drug. All energy values were computed in atomic units (a.u) and converted to electronvolts (eV) for analysis and discussion. The natural bond orbital (NBO) analysis was performed using NBO 3.0 embedded in Gaussian 16 to assess charge transfer characteristics and donor–acceptor interactions [27], [28]. Topological analysis of the electron density was carried out using the quantum theory of atoms in molecules (QTAIM) to characterize the nature and strength of intermolecular interactions. Noncovalent interaction (NCI) analysis was further applied to visualize weak interactions such as hydrogen bonding, van der Waals forces, and steric repulsion. Density of states (DOS) calculations were conducted to elucidate the influence of doping and drug adsorption on the electronic structure and sensing capabilities of the materials. All computations were performed using the Gaussian 16 package and GaussView 6.0 [29]. Visualization of molecular structures, NCI surfaces, and DOS spectra was carried out using Visual Molecular Dynamics (VMD) embedded in Multiwfn 3.8 [30] [31]

2.1 Molecular Dynamics Protocol

Molecular dynamics (MD) simulations were performed using the Forcite module implemented in Materials Studio (version 2023) to investigate the dynamic stability and interaction behavior of cimetidine with pristine and X-doped C_3N_4 surfaces (X = B, P, S, Si) [32]. Before the MD simulations, full geometry optimizations of all individual components, including pristine and doped C_3N_4 surfaces and the cimetidine molecule, were carried out to ensure energetically stable initial configurations. Amorphous cell calculations were conducted before MD simulations to generate statistically representative systems. Each amorphous cell consisted of 50 units of the respective surface material (C_3N_4, $B@C_3N_4$, $P@C_3N_4$, $S@C_3N_4$, or $Si@C_3N_4$)

View Article Online
DOI: 10.1039/D6MA00432F

and 100 cimetidine molecules, corresponding to weight fractions of 49.59113 wt% for the surface material and 50.40887 wt% for cimetidine. These configurations were used as starting points for all MD simulations.

The MD simulations were carried out in the canonical (NVT) ensemble at 298 K, regulated using a Nosé thermostat with a mass parameter of 104.799 kcal·mol^{-1}·ps^2 and a Q-ratio of 0.01. A time step of 1.0 fs was employed, and simulations were conducted for 100,000 steps, corresponding to a total simulation time of 100 ps. Additional simulation time of 500 ps was also performed for all systems, with 500,000 steps, to assess time-dependent stability and reproducibility. The Universal force field (UFF) was applied during the MD simulations, with atomic charges taken as the current charge assignments [33]. Long-range electrostatic interactions were treated using the Ewald summation method with an accuracy of 0.001 kcal·mol^{-1} and a buffer width of 2 Å. van der Waals interactions were calculated using an atom-based summation method with a cubic spline truncation, employing a cutoff distance of 12.5 Å, a spline width of 1 Å, and long-range corrections, with a buffer width of 2 Å.

2.1.1. Mean Square Displacement and Diffusion Coefficient

The translational mobility of cimetidine molecules on pristine and X-doped C_3N_4 surfaces was quantified using the mean square displacement (MSD) analysis obtained from molecular dynamics trajectories. The MSD is defined in **equation (2)** as:

$$MSD(t) = \langle |r_i(t) - r_i(0)|^2 \rangle \quad (2)$$

Where $r_i(t)$ is the position vector of the *i-th* atom or molecule at time *t*, $r_i(0)$ is the initial position vector at time *t=0*, t is the simulation time, and $\langle \ldots \rangle$ denotes an ensemble average over all selected atoms or molecules and over multiple time origins to improve statistical accuracy. The self-diffusion coefficient (D) was determined from the linear region of the MSD curve at long simulation times using the Einstein relation in **equation (3)**:

$$D = \lim_{t\to\infty} \frac{|r_i(t)-r_i(0)|^2}{6t} = \lim_{t\to\infty} \frac{MSD(t)}{6t} \quad (3)$$

Where *D* is the diffusion coefficient, the factor 6 corresponds to three-dimensional diffusion (2 × dimensionality), and the limit $t \to \infty$ ensures that the diffusive regime is reached, where the MSD increases linearly with time. In practice, the diffusion coefficient was obtained by linear fitting of the MSD versus time plot, as given in **equation (4)**:

$$D = \frac{m}{6} \quad (4)$$

View Article Online
DOI: 10.1039/D6MA00432F

Where *m* is the slope of the linear fit of the MSD as a function of time [34]. This approach enables quantitative comparison of the mobility and release behaviour of cimetidine on different graphene-based surfaces under physiological temperature conditions.

2.1.2. Radial Distribution Function (RDF)

The structural organization and spatial correlations between cimetidine molecules and the pristine or X-doped C_3N_4 surfaces were analyzed using the radial distribution function (RDF), *g(r)*. The RDF describes the probability of finding a particle at a distance r from a reference particle relative to that in an ideal homogeneous system and is defined as in **equation (5)**:

$$g(r) = \frac{1}{4\pi r^2 \rho N} \langle \sum_{i=1}^{N} \sum_{j \neq i} \delta(r - |r_i - r_j|) \rangle \qquad (5)$$

Where *r* is the radial distance between two particles, r_i and r_j are the vectors of the particles *i* and *j,* respectively, N is the total number of particles considered, ρ is the average number density of particles in the system, and δ is the Dirac delta function. In practice, *g(r)* was computed by accumulating the number of particles located within a spherical shell of thickness dr at a distance r from a reference atom or functional group and normalizing it with respect to the bulk density [35]. Peaks in the RDF indicate preferred intermolecular distances and coordination shells, providing insight into the strength and nature of interactions between cimetidine and the surface, while the decay of $g(r)$ toward unity at larger distances reflects the loss of structural correlation and the transition to bulk-like behavior.

3.0 Results and Discussion

3.1 Adsorbent Structures

The observed bond lengths and angles, as presented in **Table 1**, provide mechanistic insight into how different groups on the periodic table modulate surface reactivity and the expected behavior during cimetidine adsorption and delivery. Boron (Group 13) is small and electron-deficient; its short B–C bond (≈1.52 Å) and near-120° geometry preserve planarity and substantial orbital overlap with the host π-system, producing a localized electron-accepting center that both lowers the LUMO and increases electrophilicity. Such a site is chemically well-suited to form strong, stabilizing interactions with electron-rich moieties of cimetidine, such as lone pairs on imidazole or thioether groups, thereby promoting firm adsorption and being advantageous for loading but potentially requiring a deliberate trigger or environmental change for release. In contrast, larger dopants from Groups 14–16 (Si, P, S) impose more prolonged

View Article Online
DOI: 10.1039/D6MA00432F

X–C separations and severe angular distortions (angles ≈ 88–94°), reflecting weaker covalent overlap, greater out-of-plane character, and local lattice strain. These structural attributes tend to produce more localized, less delocalized frontier orbitals and often raise the HOMO (as seen for S) or give intermediate electrophilicity (P, Si). Mechanistically, such distorted sites can favor physisorption or weaker chemisorption modes driven by electrostatic interactions, van der Waals forces, or donor–acceptor interactions that are more reversible under physiological conditions. Thus, S- and Si-modified surfaces are likely to enable easier desorption and more controlled release kinetics, while B-doped surfaces should provide stronger retention of cimetidine. The P-doped case sits between these extremes and may be tuned for moderate binding/stability. The retention of typical N–H and C–N distances across systems suggests the framework remains chemically intact after doping. The C-N bond lengths range between 1.32 Å and 1.41 Å, which is confirmed by Asif *et al.* in their study of g-C_3N_4 delivery of lonidamine to be within the range of 1.38 Å and 1.48 Å. N-H bond lengths from the study (1.00 Å to 1.94 Å) also correlate with the present study, falling within the range of 1.01 Å to 1.02 Å as seen in **Table 1** [36].

Table 1. Optimized bond lengths and bond angles for pristine and X-doped C_3N_4 structures, showing the effect of heteroatom substitution on local geometry and surface reactivity.

Adsorbent	Bond Label	Bond length (Å)	Bond angle Label	Bond angle (Å)
C_3N_4	N_{31}-H_{32}	1.01	H_{32}-N_{31}-H_{33}	121.33
	C_4 -N_{52}	1.41	C_4 -N_{52} -C_2	120.73
	C_{15} -N_{45}	1.32	C_{15} -N_{45}-C18	117.13
B@C_3N_4	B_{54}-C_{16}	1.52	C_{16} -B_{54} -C_{14}	121.69
	C_4 -N_{52}	1.41	C_4 -N_{52} -C_2	120.89
	N_{23} -H_{24}	1.02	C_1-N_{23} -H_{24}	115.67
P@C_3N_4	P_{54}-C_{16}	1.86	C_{16}-P_{54}-C_{14}	91.01
	N_{53}-C_{10}	1.41	C_9-N_{53}-C_{10}	119.78
	N_{19}-H_{20}	1.02	C_{17}-N_{19} -H_{20}	115.02
S@C_3N_4	S_{54}-C_{15}	1.84	C_{15}-S_{54}-C_{16}	93.82
	N_{48}-C_7	1.35	N_{48}-C_7-N_{28}	116.36
	H_{32}-N_{31}	1.01	H_{32}-N_{31}-H_{33}	121.33
Si@C_3N_4	C_{15}-S_{54}	1.92	C_{15}-S_{54}-C_{14}	87.73

View Article Online
DOI: 10.1039/D6MA00432F

	N_{38}-C_3	1.32	N_{38}-C_3-N_{52}	119.01
	N_{23}-H_{24}	1.02	C_{11}-$N_{23}H_{24}$	116.95

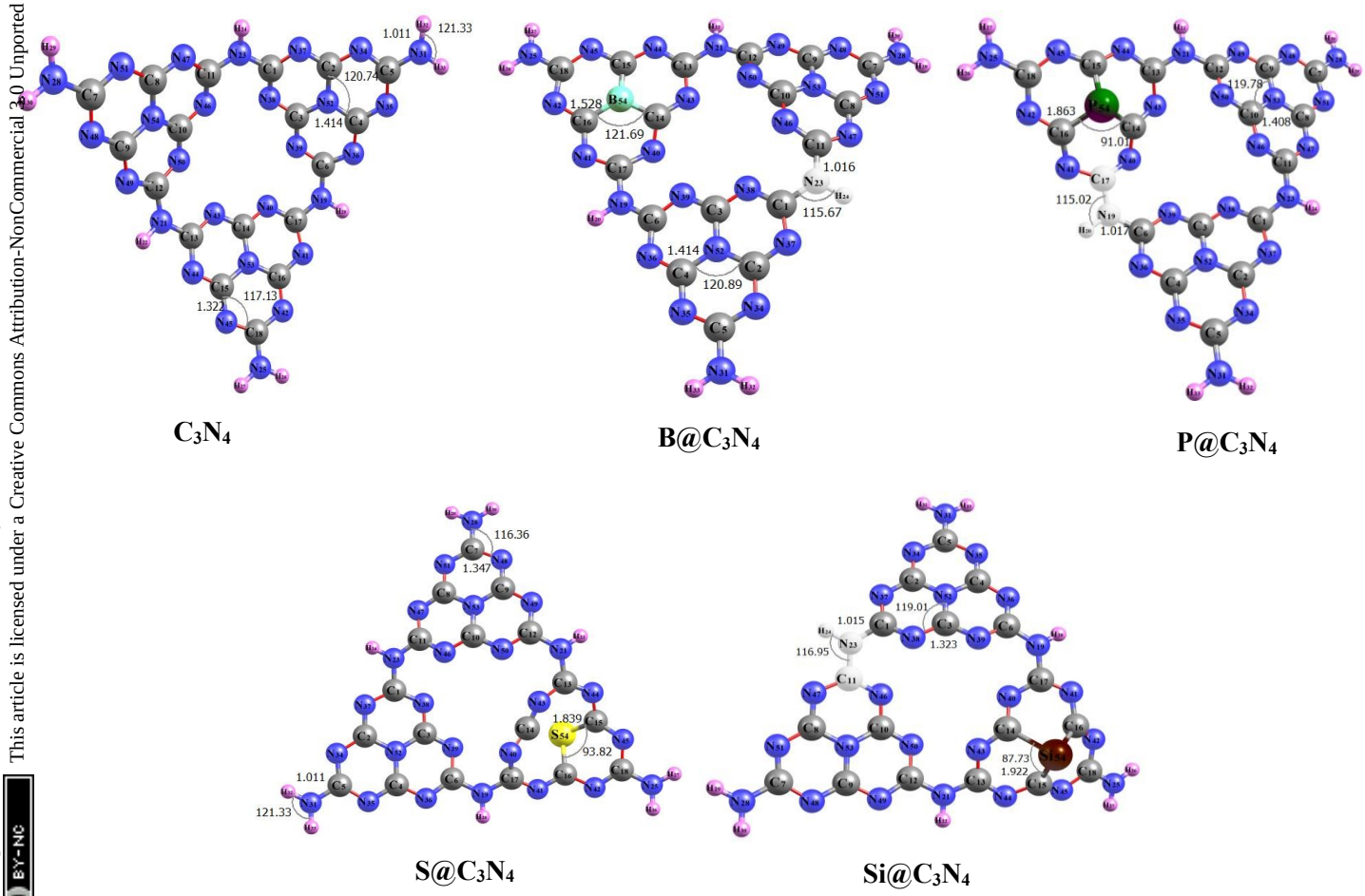

C_3N_4 $B@C_3N_4$ $P@C_3N_4$

$S@C_3N_4$ $Si@C_3N_4$

Figure 1. Optimized geometries of pristine and X-doped C_3N_4 structures, highlighting local distortions and bonding environments introduced by heteroatom substitution.

View Article Online
DOI: 10.1039/D6MA00432F

3.2 Electronic properties

3.2.1 Density of States (DOS)

The total and partial density of states (DOS and PDOS) analyses, as seen in **Figure 2 and S1** of the supporting information, provide crucial insight into the electronic structure modifications induced by dopant incorporation and drug adsorption on C_3N_4 surfaces. The pristine C_3N_4 surface exhibits a clear band gap region, with the valence band primarily dominated by nitrogen 2p orbitals and the conduction band mainly composed of carbon 2p orbitals [37]. The relatively wide separation between the valence band maximum (VBM) and conduction band minimum (CBM) reflects the intrinsic semiconducting nature of C_3N_4, consistent with its calculated energy gap from FMO analysis (3.93 eV). Upon interaction with cimetidine (Cmt), the DOS plots reveal new localized states near the Fermi level, indicating enhanced electronic coupling and charge redistribution at the interface.

Doping with heteroatoms such as B, P, S, and Si significantly modifies the DOS profile and reduces the effective band gap by introducing impurity energy levels near the Fermi level. For B@C_3N_4 and P@C_3N_4 systems, distinct peaks appear within the band gap, corresponding to dopant-induced hybridization between the B 2p/P 3p orbitals and the N 2p orbitals of the host lattice. This hybridization enhances electronic conductivity and facilitates charge transfer during adsorption. The B@C_3N_4 system shows an upward shift in the Fermi level (–8.608 eV) and higher PDOS intensity near the conduction band, signifying an increased density of unoccupied states that favor electron acceptance from cimetidine [38]. Similarly, P doping introduces shallow donor states and narrows the band gap to 2.95 eV, as reflected by the strong overlapping of P 3p and C 2p orbitals, promoting interfacial charge mobility. In contrast, S and Si dopants produce broader PDOS distributions around the Fermi level, indicating enhanced orbital delocalization and surface reactivity. The S@C_3N_4 system (E_{FL} = –5.781 eV) displays multiple overlapping states between sulfur 3p and nitrogen 2p orbitals, which contribute to increased electronic activity and stronger physisorption of the drug. Si@C_3N_4, with its moderate Fermi level (–8.254 eV), demonstrates a more balanced electronic configuration, where Si 3p–C 2p hybridization leads to uniform charge distribution and controlled adsorption

View Article Online
DOI: 10.1039/D6MA00432F

behavior. This aligns with the QTAIM and adsorption analyses, which identified Si doping as a stabilizing modification that supports sustained, reversible drug binding.

Upon complex formation with cimetidine, all doped systems exhibit additional DOS peaks near the Fermi level, indicating strong orbital overlap and charge redistribution between the drug molecule and the surface. The intensity of these states varies with dopant type, with B- and Si-doped systems showing more pronounced hybrid peaks, confirming effective electronic interaction and charge delocalization. P@C_3N_4, while exhibiting the highest state density, shows excessive localization that may hinder charge relaxation and contribute to its positive adsorption energy. S doping maintains moderate interaction strength with enhanced electronic responsiveness due to the shallow impurity states near the Fermi level, which facilitate electron hopping during adsorption–desorption cycles. The DOS analysis demonstrates that dopant incorporation effectively tailors the electronic structure of C_3N_4, reducing its band gap and improving charge transfer efficiency with cimetidine. The observed shifts in Fermi energy and emergence of hybrid states signify enhanced surface conductivity and sensitivity, key properties for drug sensing and release. Among the investigated systems, B- and Si-doped C_3N_4 exhibit the most favorable DOS features, combining strong drug–surface coupling with stable electronic configurations, whereas S doping promotes faster response behavior due to increased surface reactivity.

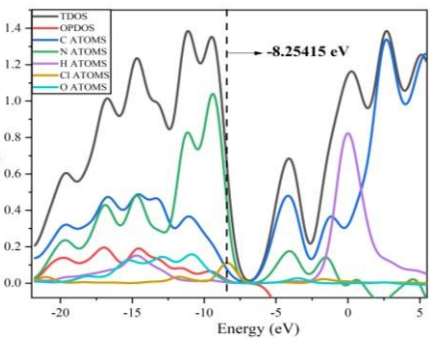

Vfs-C_3N_4

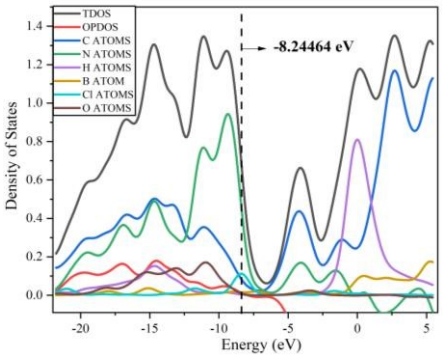

Vfs-B@C_3N_4

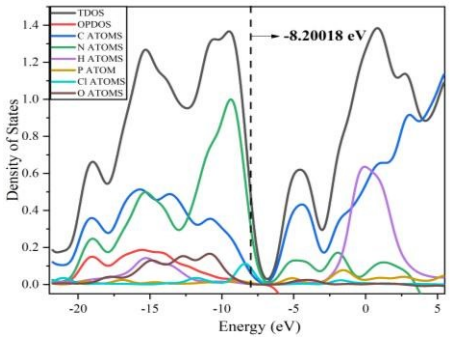

Vfs-P@C_3N_4

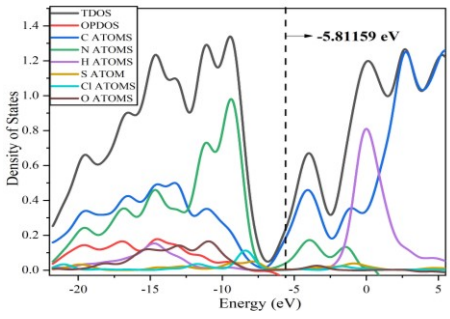

Vfs-S@C_3N_4

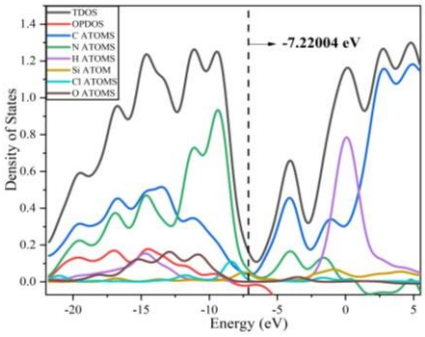

Vfs-Si@C_3N_4

View Article Online
DOI: 10.1039/D6MA00432F

Figure 2. Projected density of states (PDOS) of Cmt-surface complexes, showing electronic modifications induced by drug adsorption and the emergence of new states near the Fermi level.

3.2.2 Natural Bond Orbital Analysis (NBO)

The Natural Bond Orbital (NBO) second-order perturbation analysis reveals distinct donor–acceptor (stabilizing) interactions that rationalize the dopant-dependent reactivity of the C_3N_4 materials as recorded in **Table S1**. For the pristine framework and B-doped material the dominant transitions are lone-pair → π* (LP→π*) interactions with moderate stabilization energies ($E^{(2)}$ ≈ 20–22 kcal·mol^{-1}, energy gaps ≈0.35–0.36 a.u., F(i,j) ≈ 0.077–0.081 a.u.), consistent with modest delocalization of nitrogen lone pairs into the anti-bonding π* manifold of the network. By contrast, P- and S-substituted sites show vast LP→π* stabilization energies (P@C_3N_4: $E^{(2)}$ ≈ 100–107 kcal·mol^{-1}; S@C_3N_4: $E^{(2)}$ ≈ 85–101 kcal·mol^{-1}) associated with much smaller donor–acceptor energy gaps (≈0.14–0.15 a.u. for P; ≈0.08–0.10 a.u. for S) and larger Fock matrix couplings (F(i,j) ≈ 0.12 a.u.). These large $E^{(2)}$ values point to powerful dative/hyperconjugative interactions at P and S centers, effectively indicating substantial charge delocalization from lone pairs into the framework's antibonding orbitals and (for P) possible partial covalent/dative character [39]. Silicon substitution shows the weakest stabilization overall (Si@C_3N_4: $E^{(2)}$ ≈ 9–11 kcal·mol^{-1} for the main interactions) and includes an LP→σ* entry (9.29 kcal·mol^{-1}), suggesting that Si insertion yields smaller orbital overlap with the π-system and more localized, weaker interactions. In short, the NBO data indicate that P and S greatly enhance donor→acceptor coupling within the doped lattice, B gives moderate delocalization, while Si yields the weakest perturbation to the π network.

When cimetidine (Cmt) is included, the NBO interactions between drug and surface quantify the direction and strength of charge transfer and therefore the nature of adsorption. Significant LP(N_drug)→π*(surface) stabilizations appear for Cmt-B@C_3N_4 ($E^{(2)}$ ≈ 46.6 kcal·mol^{-1}, F ≈ 0.129 a.u., ΔE ≈ 0.43 a.u.) and Cmt-C_3N_4 ($E^{(2)}$ ≈ 45.9 kcal·mol^{-1}), indicating robust electron donation from the drug's nitrogen lone pairs into acceptor orbitals on the surface, a hallmark of strong chemisorptive or strongly stabilized donor–acceptor complexes. Cmt-S@C_3N_4 and Cmt-Si@C_3N_4 show even larger single-entry stabilizations (e.g., Cmt-Si: $E^{(2)}$ ≈ 111.9 kcal·mol^{-1}; Cmt-S: ≈108.2 kcal·mol^{-1} for the leading LP→π* transitions) and additional significant π→LP or LP→LP couplings, implying the formation of very strongly stabilized interfacial states (high degree of charge transfer and possibly partial covalent character). Conversely, weaker interactions ($E^{(2)}$ < ~30 kcal·mol^{-1}) such as those seen in Si@C_3N_4 intrinsic entries reflect physisorption-like or weakly chemisorbed behavior.

View Article Online
DOI: 10.1039/D6MA00432F

Implications for drug-delivery design follow directly. High stabilization energies ($E^{(2)} \gtrsim 40$–100 kcal·mol^{-1}), observed for P- and S-doped sites and for several Cmt-X complexes, suggest chemisorptive or strongly dative interactions that will enhance loading capacity and immobilize cimetidine effectively but may impede rapid release without an external trigger (pH change, competitive ligand, redox). Moderate $E^{(2)}$ values (≈20–50 kcal·mol^{-1}), typical of B-doped and vacancy-bearing systems, indicate strong but potentially reversible donor–acceptor binding, possibly optimal for sustained release. Low $E^{(2)}$ (< ≈15 kcal·mol^{-1}), as seen for intrinsic Si entries, suggests weak physisorption favorable to rapid release but poorer initial loading.

3.2.2.1 Mulliken Population Analysis

To gain further insight into the amount of electronic interaction and charge redistribution between cimetidine and pristine/doped C_3N_4 surfaces, Mulliken population analysis has been performed, which is summarized in **Table S2**. The analysis shows the noticeable variation of the atomic charge of cimetidine on the adsorption, changing the charge of the adsorbent surfaces, which indicates the occurrence of interfacial charge transfer between the drug molecule and the surfaces of the adsorbent. The total Mulliken charge of cimetidine stays neutral (0.000 e), while for cimetidine on the different surfaces, measurable charge redistribution can be seen. The clean C_3N_4 surface gives a net charge of +0.012 e to the adsorbed cimetidine, suggesting somewhat donating an electron from the drug to the surface. The total charges are +0.068 e and +0.075 e for B@C_3N_4 and Si@C_3N_4, respectively, indicating a more pronounced charge transfer. The positive values indicate that cimetidine can donate electron density to the electron-deficient boron- and silicon-doped surfaces, which is in accordance with the increased electrophilicity and adsorption stabilization found from the frontier molecular orbital and adsorption energy analyses. On the contrary, the P@C_3N_4 system has a small negative total charge (−0.011 e), which suggests weak back-donation of electron density from the surface of the phosphorus doped to cimetidine. This behavior is in line with the negative adsorption energy and lower adsorption stability of P@C_3N_4, suggesting that the electronic coupling between the drug and the surface is not particularly strong. The charge transfer (+0.004 e) between the S@C_3N_4 system is very small, indicating that interactions between the two are mostly weak physisorption forces, mediated primarily through dispersion and electrostatic forces.

View Article Online
DOI: 10.1039/D6MA00432F

In the cimetidine molecule, there is considerable redistribution of charge at the atomic level, which is seen in the oxygen and the nitrogen atoms in the heteroatom-functional groups. The P@C_3N_4 complex, for instance, is significantly more negative for O21 (−0.339 e) than isolated cimetidine (−0.172 e), showing localized polarization effects because of phosphorus doping. Likewise, the difference in the charges of N19, N22, O31, and neighbouring hydrogen atoms indicates that the polar heteroatoms of cimetidine are the major sites of adsorption by hydrogen bonding and donor–acceptor interactions. In conclusion, the Mulliken population analysis further corroborates the moderate charge transfer and electronic redistribution occurring during cimetidine adsorption on pristine and doped C_3N_4 surfaces. The greater charge transfer in B@C_3N_4 and Si@C_3N_4 suggests their higher adsorption affinity and interfacial interaction, while the small charge transfer in P@C_3N_4 is consistent with its low adsorption capacity.

3.2.3 Chemical Quantum Descriptors

The chemical tailoring of g-C_3N_4 by heteroatom doping with B, P, S, and Si, elements originating from Groups 13, 15, 16, and 14 of the periodic table, respectively, profoundly alters the electronic structure and reactivity of the material as recorded in **Table 2**. The pristine C_3N_4 surface exhibits an energy gap of 3.934 eV, a dipole moment of 4.525 Debye, and an electrophilicity index of 4.683 eV. These values are in good agreement with those reported by Asif *et al.,* who obtained corresponding values of 3.88 eV, 1.82 Debye, and 4.46 eV using the DFT/B3LYP/6-31G* level of theory. The slight variations, particularly in the dipole moment, can be attributed to differences in exchange–correlation functionals, basis sets, and model geometries, which are known to influence charge distribution and polarization effects [36]. Boron (Group 13) is electron-deficient relative to carbon and nitrogen; when substituted into the C_3N_4 lattice, it introduces vacant p orbitals that withdraw electron density from the framework [7]. This creates localized positive centers and significantly lowers the LUMO energy, thereby narrowing the band gap (2.12 eV for B@C_3N_4) and enhancing electrophilicity ($\omega \approx 11.7$ eV). The combination of boron doping with a surface vacancy (Cmt-B@C_3N_4) further amplifies this effect, producing the smallest gap (≈2.02 eV) and the highest electrophilicity ($\omega \approx 13.7$ eV). Such strong electron-accepting ability suggests that boron-modified g-C_3N_4 can readily interact with electron-rich regions of cimetidine (notably the imidazole and thioether moieties), promoting charge transfer and robust adsorption, which are desirable for efficient drug immobilization and controlled release.

In contrast, sulfur (Group 16) possesses a lower electronegativity and larger atomic size, donating electron density to the network and raising the HOMO level (–4.379 eV for S@C_3N_4).

View Article Online
DOI: 10.1039/D6MA00432F

This behavior yields the narrowest energy gap (≈2.00 eV) but a lower electrophilicity (ω ≈ 5.69 eV), signifying enhanced donor character and softer reactivity. S-doping therefore favors electron donation from the surface to the drug, which could stabilize adsorption via donor–acceptor or π–π* interactions if the drug's LUMO is sufficiently low-lying. Phosphorus (Group 15) and silicon (Group 14) exhibit intermediate properties. Phosphorus, being less electronegative than nitrogen but capable of forming hypervalent bonding, slightly reduces the gap (2.73 eV) and provides moderate electrophilicity (ω ≈ 7.66 eV), implying balanced donor–acceptor behavior. Silicon, isoelectronic with carbon but more electropositive, induces lattice distortion and partial charge delocalization, again lowering the gap (2.77 eV) while maintaining good chemical stability (η ≈ 1.39 eV).

When complexed with cimetidine (Cmt-X@C_3N_4 systems), all doped surfaces show reduced band gaps and modified electrophilicity compared to pristine C_3N_4, confirming strong electronic coupling between the drug and the tailored carrier. The B- and P-doped complexes exhibit the most pronounced enhancement in ω, indicating efficient charge transfer and high drug affinity. Conversely, the S- and Si-doped surfaces, with their elevated HOMO levels, are expected to promote facile electron back-donation that may weaken binding, facilitating easier drug desorption under physiological conditions. The periodic nature of the dopants dictates the balance between reactivity and stability: early-group elements such as B create electron-deficient, highly reactive surfaces optimal for strong adsorption, whereas later-group dopants like S yield more stable, electron-rich surfaces favorable for controlled release. These tunable electronic properties imply that doping provides a rational strategy to modulate drug–carrier interactions in graphene-like C_3N_4 systems, enabling the design of optimized nanocarriers for targeted and sustained cimetidine delivery.

View Article Online
DOI: 10.1039/D6MA00432F

Table 2. Frontier molecular orbital (FMO) parameters and quantum chemical descriptors for pristine and X-doped C_3N_4 (X = B, P, S, Si), including HOMO–LUMO energies, band gaps, ionization potential (IP), electron affinity (EA), chemical hardness (η), electronegativity (χ), and electrophilicity index (ω).

Materials	**E_{HOMO} (eV)**	**E_{LUMO} (eV)**	**Eg (eV)**	**η (eV)**	***x*** **(eV)**	**Dipole (Debye)**	**ω (eV)**
C_3N_4	-6.259	-2.325	3.934	1.967	4.292	4.525	4.683
B@C_3N_4	-6.046	-3.922	2.124	1.062	4.984	2.244	11.695
P@C_3N_4	-5.937	-3.208	2.730	1.365	4.572	2.614	7.660
S@C_3N_4	-4.379	-2.375	2.004	1.002	3.377	1.335	5.689
Si@C_3N_4	-5.805	-3.032	2.773	1.387	4.418	2.574	7.039
Cmt	-6.667	-1.794	4.874	2.437	4.230	4.343	3.672
Cmt-C_3N_4	-6.140	-2.523	3.617	1.809	4.331	7.284	5.187
Cmt-B@C_3N_4	-6.280	-4.256	2.024	1.012	5.268	5.570	13.713
Cmt-P@C_3N_4	-6.480	-3.527	2.954	1.477	5.004	4.282	8.477
Cmt-S@C_3N_4	-4.503	-2.500	2.004	1.002	3.501	4.889	6.119
Cmt-Si@C_3N_4	-5.803	-3.113	2.690	1.345	4.458	5.562	7.387

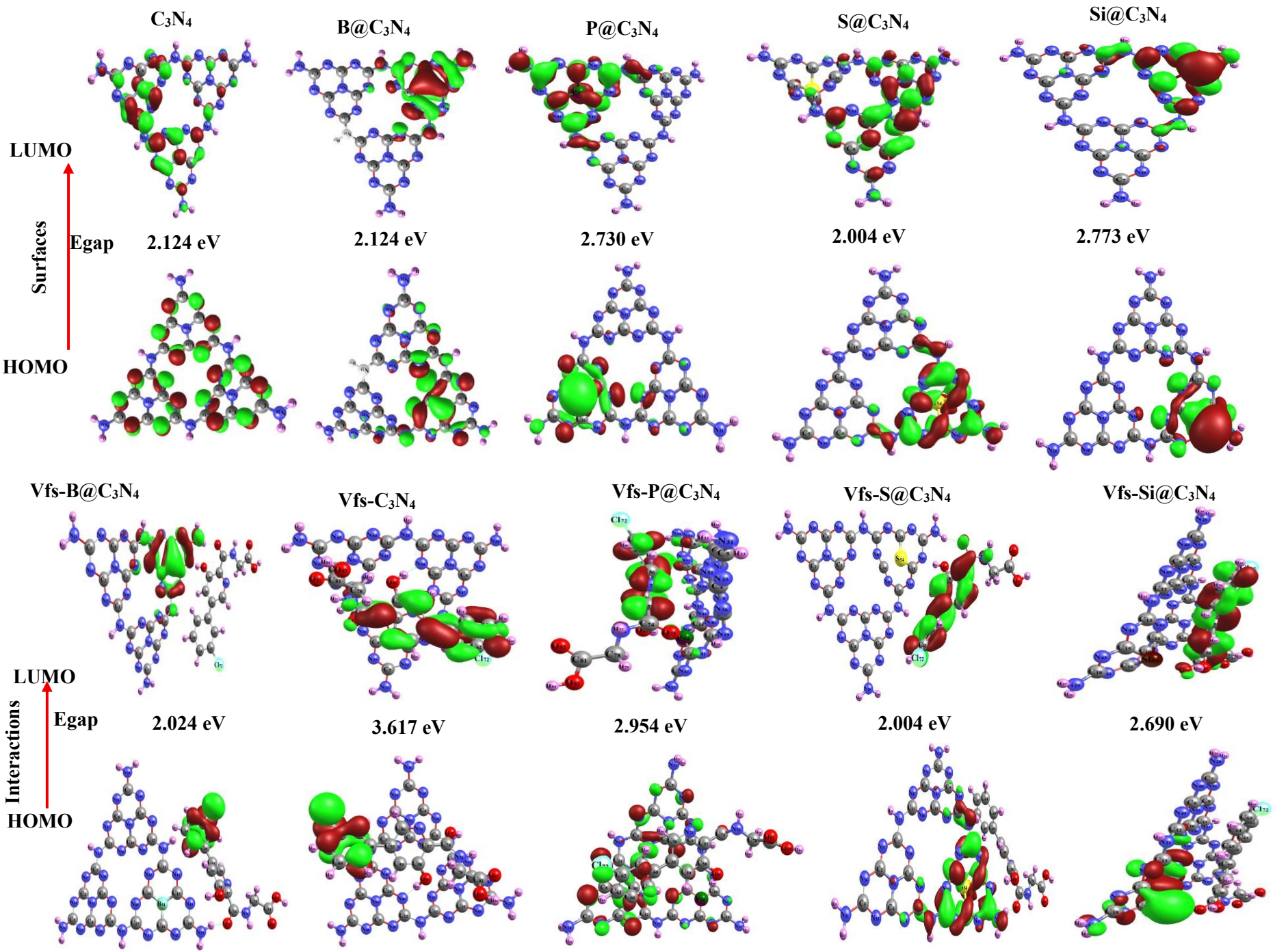

View Article Online
DOI: 10.1039/D6MA00432F

Figure 3. HOMO–LUMO molecular orbital distributions for cimetidine (Cmt) adsorbed on pristine and X-doped C_3N_4 surfaces (X = B, P, S, Si). The plots illustrate changes in frontier orbital localization, charge redistribution, and orbital overlap upon adsorption, highlighting the influence of heteroatom doping on electronic reactivity and interaction strength.

3.3 Adsorption Studies

The adsorption energies (E_{ads}) of cimetidine (Cmt) on pristine and X-doped g-C_3N_4 surfaces (X = B, P, S, Si) provide information on the strength and nature of drug–carrier interactions. Negative E_{ads} values indicate exothermic adsorption and thermodynamically favorable binding, whereas positive values suggest weak or unstable association. As summarized in **Table 3**, the calculated adsorption energies range from –3.784 eV (Cmt-C_3N_4) to –3.020 eV (Cmt-P@C_3N_4), confirming spontaneous and stable adsorption of cimetidine onto the carrier surface, suggesting effective drug loading without structural instability. Importantly, the interaction energies fall within the optimal window for noncovalent drug–carrier binding, where the drug is sufficiently retained during circulation yet remains releasable at the target site.[40].

Pristine g-C_3N4 (Cmt-C_3N4) exhibits the strongest adsorption (−3.755 eV), indicating a high affinity toward cimetidine. This strong interaction implies excellent loading capacity and protection of the drug from premature degradation; however, it may also lead to slower release kinetics, which could necessitate external stimuli (pH variation or competitive biomolecules) to ensure efficient drug release. In contrast, heteroatom doping systematically moderates the adsorption strength, thereby tuning the release behavior while maintaining adequate stability.

Among the doped systems, Si- and B-doped g-C_3N_4 show intermediate adsorption energies (−3.320 and −3.238 eV, respectively), representing a favorable balance between drug retention and controlled release. These systems are particularly attractive for sustained-release formulations of cimetidine, where prolonged therapeutic levels are required. This correlates well with the NBO and electrophilicity results. The B-doped surface, which displayed the highest electrophilicity ($\omega \approx 13.7$ eV for Cmt-B@C_3N_4) and substantial LP → π* charge-transfer stabilization ($E^{(2)} \approx 46$ kcal mol^{-1}), acts as a strong electron acceptor toward the drug's lone-pair donor sites. This strong donor–acceptor interaction stabilizes the adsorbed complex without forming overly rigid bonds, a desirable feature for maintaining drug attachment while allowing eventual release. In contrast, the Si-doped system exhibits a comparable adsorption energy but somewhat weaker charge-transfer stabilization, consistent with their higher HOMO levels and lower electrophilicity, behaviors that favor electron donation from the surface to the

View Article Online
DOI: 10.1039/D6MA00432F

drug, resulting in more reversible adsorption. S- and P-doped g-C_3N_4 display slightly weaker interactions (−3.075 and −3.020 eV), which suggests easier desorption of cimetidine from the surface. Such behavior is advantageous for rapid or on-demand drug release, reducing the risk of drug entrapment and enhancing bioavailability at the target site. The results demonstrate that heteroatom-doped g-C_3N_4 provides a tunable platform for cimetidine delivery, where adsorption strength, and consequently drug-release kinetics, can be rationally adjusted through surface modification. Pristine g-C_3N_4 is best suited for high loading and prolonged retention, while doped variants, particularly Si- and B-doped systems, offer optimized performance for controlled drug delivery.

In this study, the adsorption energies for cimetidine on the doped C_3N_4 systems (from −3.02 to −3.76 eV) are quite high and strong, and the adsorption energy values are larger than those of the conventional carbon-based systems. A comparative table has been provided in **Table S3.** The adsorption energies are typically between −0.6 and −2.5 eV for graphene oxide systems, depending on the functionalization and the drug type, and are dominated by hydrogen bonding and van der Waals forces [41]. For carbon nanotube-based systems, the strength of adsorption is usually weaker, with adsorption being more often of non-covalent π–π interaction, and less tunable than with doped heteroatom frameworks, and weaker than in the latter [42]. Metal–organic frameworks (MOFs) may provide similar or even higher adsorption energies via coordinative binding sites, but they may not be structurally stable in aqueous and physiological environments, thereby limiting practical biomedical use. The doped g-C_3N_4 systems studied here, in contrast, offer high adsorption strength, structural robustness and tunable electronic properties, which make them potential candidates for applications in drug delivery towards strong drug loading and controlled delivery.

Table 3. Adsorption energies (E_{ads}) of cimetidine (Cmt) on pristine and doped C_3N_4 systems, illustrating the relative binding strengths and stability of drug–surface complexes.

Compounds	E_{INT} (a.u)	E_{CMT} (a.u)	E_{SUR} (a.u)	E_{ads} (a.u)	E_{ads} (eV)
Cmt-B@C_3N_4	-3548.316	-1409.883	-2138.314	-0.119	-3.238
Cmt-C_3N_4	-3578.300	-1409.883	-2168.279	-0.139	-3.755
Cmt-P@C_3N_4	-3668.990	-1409.883	-2259.000	-0.111	-3.020
Cmt-S@C_3N_4	-3921.552	-1409.883	-2511.556	-0.113	-3.075
Cmt-Si@C_3N_4	-3812.857	-1409.883	-2402.852	-0.123	-3.320

View Article Online
DOI: 10.1039/D6MA00432F

3.4 Visual Studies

3.4.1 Quantum Theory of Atoms in Molecules

The Quantum Theory of Atoms in Molecules (QTAIM) provides deeper insight into the electronic characteristics and bonding nature between cimetidine (Cmt) and the doped g-C_3N_4 surfaces. The key topological parameters, including the electron density at the bond critical point ($\rho(r)$), its Laplacian ($\nabla^2\rho$), kinetic energy density (G(r)), potential energy density (V(r)), and total energy density (H(r)), are used to differentiate between covalent and non-covalent interactions as presented on **Table S4**. In general, high $\rho(r)$ and negative $\nabla^2\rho$ values indicate shared-shell (covalent) interactions, while lower $\rho(r)$ and positive $\nabla^2\rho$ values correspond to closed-shell interactions such as hydrogen bonding, van der Waals forces, or electrostatic contacts [43], [44].

Across all investigated systems, the $\rho(r)$ values (0.11–0.94 a.u.) and $\nabla^2\rho$ (0.11–0.92 a.u.) fall within the range typical of intermediate closed-shell interactions, signifying that adsorption predominantly occurs through electrostatic and hydrogen-bond-mediated physisorption rather than full covalent bonding. This conclusion aligns well with the moderate adsorption energies (≈ –3 eV) observed in the adsorption analysis, suggesting favorable and reversible binding suitable for drug delivery. In the pristine Cmt-C_3N_4 complex, relatively high electron densities (ρ = 0.67 a.u. at C_{18}–O_{82}) combined with low positive Laplacian ($\nabla^2\rho$ = 0.26 a.u.) indicate partially polarized covalent interactions between the oxygen site of cimetidine and the nitrogen-rich surface of C_3N_4. The negative H(r) (–0.43 a.u.) and G(r)/V(r) < 1 confirm a moderate degree of covalent character within an overall electrostatic interaction framework. Hydrogen bonds such as N_{19}–O_{75} and N_{50}–H_{86}, with lower electron densities (≈ 0.1–0.5 a.u.), reflect weaker but stabilizing electrostatic contacts that contribute to surface anchoring without causing irreversible adsorption.

Upon boron doping, the system exhibits enhanced electron delocalization and increased charge transfer between the drug and surface. The B-containing complex shows higher $\rho(r)$ values (0.59–0.67 a.u.) and slightly lower G(r)/V(r) ratios (~0.2–0.3), indicating the presence of moderately covalent character superimposed on the electrostatic framework. The negative H(r) values confirm partial electron sharing, consistent with the NBO results that showed strong LP→π* charge transfer transitions. These features suggest that B-doping strengthens the surface–drug interaction while maintaining reversibility, a desirable property for controlled drug delivery applications. Phosphorus doping, on the other hand, displays the highest $\rho(r)$

View Article Online
DOI: 10.1039/D6MA00432F

values (0.82–0.94 a.u.) and notably negative H(r), signifying significant charge accumulation at the bond critical points. However, the low G/V ratios (~0.3) and highly localized electron densities indicate excessive polarization, which can destabilize the adsorption complex through increased electronic repulsion. This finding explains the anomalous positive adsorption energy observed for the P-doped system, reflecting reduced thermodynamic favorability despite strong local electronic interactions. Sulfur-doped C_3N_4 demonstrates intermediate behavior, with $\rho(r)$ values ranging from 0.26 to 0.67 a.u. and positive $\nabla^2\rho$ values indicative of hydrogen-bond-dominated closed-shell interactions. The H_{27}–O_{75} and N_{48}–H_{69} contacts exemplify this character, showing moderate electron densities and positive Laplacian values typical of electrostatic stabilization. The electron localization function (ELF) values (0.4–0.7) reveal localized electron pairs around sulfur and nitrogen centers, implying multiple weak interactions that enhance overall adsorption stability. This correlates with the moderate adsorption energy (–3.09 eV), confirming that S-doping promotes reversible, non-destructive adsorption favorable for rapid or pH-triggered drug release. The Si-doped surface shows mixed covalent–polar interactions, with $\rho(r)$ values between 0.57–0.86 a.u. and $\nabla^2\rho$ values of 0.16–0.20 a.u., indicating stable yet reversible binding between cimetidine and the Si-modified surface. The Si–H86 contact (ρ = 0.86 a.u.) shows partial electron sharing and a moderate G/V ratio (~0.55), while the negative H(r) confirms weak chemisorption. The ELF values (~0.15) and negative λ_2 values suggest localized electron accumulation around the Si dopant, improving adsorption stability without excessive binding.

Boron and silicon doping enhance charge delocalization and lead to optimal adsorption strength and reversibility, suitable for sustained or controlled release of cimetidine. Sulfur doping favors weaker, fast-releasing interactions, whereas phosphorus doping induces excessive localization, leading to instability and poor adsorption efficiency. The pristine C_3N_4 surface offers a balanced interaction profile, but doping, particularly with B and Si, significantly improves drug–carrier compatibility and tunability of binding strength.

View Article Online
DOI: 10.1039/D6MA00432F

3.4.2 Non-Covalent Interactions

The Non-Covalent Interaction (NCI) analysis provides valuable insight into the nature, strength, and distribution of intermolecular forces governing the adsorption of cimetidine (Cmt) on pristine and doped C_3N_4 surfaces. The colored isosurfaces represent the types of interactions occurring at the interface, where blue regions correspond to attractive interactions such as hydrogen bonding, green regions indicate weak van der Waals (vdW) or dispersive forces, and red regions denote steric repulsion or strong electrostatic effects [45]. Across all systems, mixed interaction zones are observed, reflecting a balance between physisorption and localized chemisorptive contributions depending on the dopant type. For the pristine Cmt@C_3N_4 complex, the interaction is dominated by green regions, suggesting that adsorption primarily occurs through van der Waals and π–π stacking interactions between the aromatic rings of cimetidine and the conjugated C_3N_4 surface. This is consistent with the moderate adsorption energy (–3.25 eV) and limited charge transfer identified in the adsorption and QTAIM analyses, confirming a physisorption-driven mechanism.

Upon doping, distinct modifications in the NCI surfaces are observed, reflecting enhanced interaction diversity and charge redistribution. The Cmt-B@C_3N_4 system shows prominent blue regions localized around the N–H and O–H groups of cimetidine and adjacent nitrogen atoms of the doped surface, indicating strong hydrogen bonding and attractive electrostatic interactions. The presence of mild red contours near the B dopant suggests localized polarization due to charge accumulation, enhancing adsorption stability without significant steric hindrance. In the Cmt-P@C_3N_4 complex, large patches of both blue and red isosurfaces appear around the P dopant and the drug molecule, implying competitive effects of strong hydrogen bonding and electrostatic repulsion. This dual behavior corresponds to the high adsorption energy (positive E_{ads}) and significant charge redistribution, indicating that while P doping increases chemical reactivity, it can also induce localized electronic strain and repulsive forces. The Cmt-S@C_3N_4 system displays a predominance of green and light blue regions, highlighting balanced dispersive and hydrogen-bonding interactions. The sulfur dopant contributes to surface polarization, improving adsorption via weak donor–acceptor interactions between the S atom and N–H groups of the drug. These characteristics correspond with the moderate adsorption energy (–3.08 eV) and controlled charge transfer observed earlier, signifying a favorable physisorption–chemisorption hybrid mechanism ideal for reversible sensing or release. For the Cmt-Si@C_3N_4surface, extensive blue-green hybrid zones are observed across the interface, especially near Si–N and Si–H coordination sites. This indicates

synergistic effects of hydrogen bonding and dispersive interactions, supporting stable yet flexible adsorption. Minor red regions near the Si dopant correspond to slight steric congestion due to its larger atomic radius, which slightly modifies local electron density without destabilizing the system. The strong overlap between cimetidine's heteroatoms and the Si-modified C_3N_4 framework suggests efficient charge delocalization, consistent with QTAIM evidence of mixed covalent–electrostatic bonding and moderate adsorption energy (–3.35 eV).

The NCI analysis reveals that dopant incorporation effectively tunes the non-covalent landscape of the C_3N_4 surface. B and Si dopants promote stronger hydrogen bonding and charge stabilization, while S doping enhances vdW contributions, and P doping introduces localized electronic perturbations.

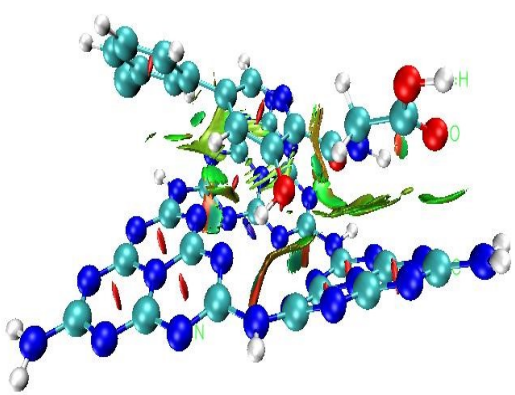

Vfs-C_3N_4

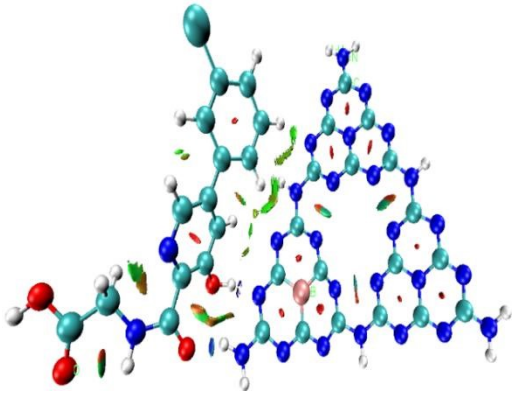

Vfs-B@C_3N_4

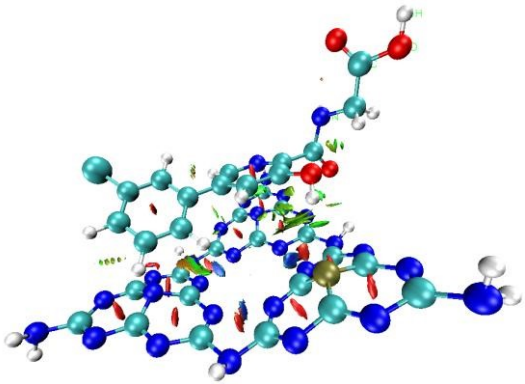

Vfs-P@C_3N_4

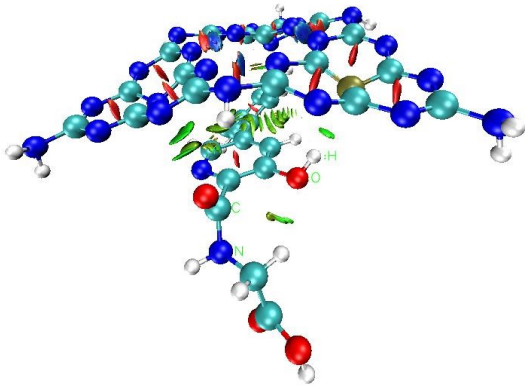

Vfs-S@C_3N_4

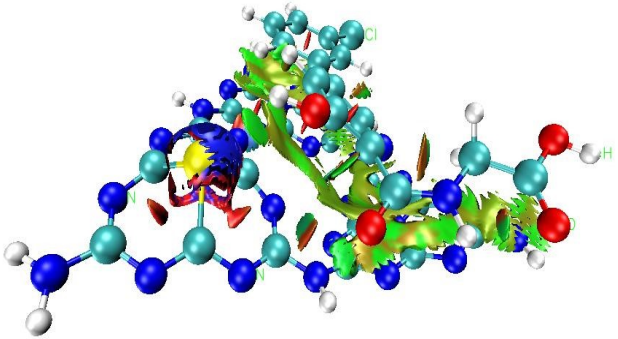

Vfs-Si@C_3N_4

Blue represents attractive or hydrogen interaction.

Green represents Van der Waal force of interaction or dispersive force

Red represents strong electrostatic interaction or steric repulsion

View Article Online
DOI: 10.1039/D6MA00432F

Figure 4. Noncovalent interaction (NCI) plots for Cmt adsorbed on pristine and doped C_3N_4, with isosurfaces visualizing attractive interactions (blue), dispersive interactions (green), and steric repulsion (red).

3.5 Sensor mechanisms

The sensor performance of the doped C_3N_4 systems toward cimetidine was further investigated by analyzing back-donation, work function, charge transfer (Qt), the fraction of electron transfer, and dipole moment. These parameters provide critical insights into how electron exchange between the drug molecule (Cmt) and the adsorbent surface governs sensing sensitivity and adsorption–desorption dynamics. In general, the direction and magnitude of charge transfer reflect the degree of electronic interaction. At the same time, the work function determines the surface's electronic response and its ability to act as an active sensing platform. The back-donation values range from –0.25 to –0.45, indicating that electron feedback from the surface to the adsorbate is limited and that the dominant charge flow is from cimetidine toward the doped surfaces. This unidirectional charge transfer is consistent with the donor–acceptor nature of the systems observed in the NBO and QTAIM analyses [46]. Among the systems, the pristine Cmt-C_3N_4 complex exhibits a relatively high back-donation value (–0.45), indicating greater orbital overlap between the drug molecule and the undoped surface. However, the introduction of dopants modifies the local charge density, resulting in different extents of charge redistribution and interfacial polarization.

The work function (Φ) values exhibit notable variation with doping type, ranging from 3.501 eV in S@C_3N_4 to 5.268 eV in B@C_3N_4. A lower work function corresponds to easier electron emission and higher surface reactivity, whereas a higher value suggests stronger electron confinement [47]. The S-doped system, with the lowest work function, is expected to be more electronically active and responsive to external stimuli, which enhances its potential as a fast-response drug sensor. In contrast, the B- and P-doped systems exhibit elevated work functions (5.268 eV and 5.004 eV, respectively), indicating improved electronic stability and a reduced tendency for spontaneous charge loss, properties beneficial for sustained or controlled sensing and drug release. The pristine C_3N_4 surface exhibits an intermediate work function (4.331 eV), while Si-doping (4.458 eV) slightly increases it, reflecting a subtle enhancement in charge retention and carrier response.

The charge transfer (Q_t) values further illustrate the dopant-induced modulation of electronic exchange. Negative Q_t values (e.g., –0.11365 e for B@C_3N_4 and –0.09286 e for Si@C_3N_4)

View Article Online
DOI: 10.1039/D6MA00432F

indicate charge transfer from the drug to the adsorbent, confirming that the doped surfaces act as electron acceptors [48]. The only positive Qt observed for P@C_3N_4 (+1.93 e) suggests an opposite transfer direction, consistent with the strong electron-donating nature of phosphorus, which pushes electron density toward the cimetidine molecule. This excessive charge donation, combined with its high work function, explains the less favorable adsorption energy and potential instability observed earlier. The fraction of electron transfer values (–0.12 to –0.48) reveals that B- and Si-doped systems facilitate more efficient electron exchange, enhancing their electrical sensitivity and making them promising candidates for real-time sensing of cimetidine adsorption and release.

The dipole moment (μ) values, ranging from 4.89 to 7.28 D, reflect the degree of interfacial polarization resulting from charge redistribution upon adsorption [49]. The pristine C_3N_4 complex displays the highest dipole moment (7.28 D), indicating strong dipolar alignment between the drug molecule and the surface. However, doping generally reduces μ, suggesting that the dopant atoms promote more uniform charge distribution and mitigate localized polarization. The relatively balanced dipole moments of the B- and Si-doped systems (5.57 and 5.56 D, respectively) imply an optimal balance between electronic sensitivity and stability, reinforcing their suitability as responsive yet controllable drug-sensing materials.

The sensor mechanism analysis demonstrates that doping effectively tunes the electronic response of C_3N_4 toward cimetidine. Sulfur doping enhances surface reactivity by reducing the work function and increasing the electron mobility, making it ideal for quick-response detection. Boron and silicon doping strengthen charge delocalization and maintain stable yet sensitive electronic interfaces, supporting controlled sensing and drug-release kinetics. In contrast, phosphorus doping induces excessive electron donation and polarization, reducing sensing stability.

View Article Online
DOI: 10.1039/D6MA00432F

3.6 Monte Carlo Molecular Dynamics

Molecular dynamics (MD) simulations were performed to evaluate the structural stability, energetic convergence, and thermal equilibration of cimetidine (Cmt) adsorbed on pristine and X-doped C_3N_4 surfaces (X = B, P, S, and Si). The simulations were carried out under the NVT ensemble at 298 K for two time scales, 100 ps and 500 ps, and the resulting energetic parameters are summarized in **Tables S5 and S6**, respectively. The corresponding temperature evolution profiles are illustrated in **Figure 5**.

At 100 ps (**Table S5**), all systems exhibit a rapid relaxation from their initial configurations, as evidenced by the convergence of total and potential energies toward stable average values. The kinetic energies for all complexes remain close to ~5239 kcal/mol, consistent with the target temperature of 298 K and indicating proper thermostat functioning. Minor fluctuations observed in total and potential energies, particularly for the Cmt-P@C_3N_4 system, are associated with initial structural rearrangements and stronger host–guest interactions. Still, these variations stabilize as the simulation progresses. The temperature profiles in **Figure 5(a)** further confirm this behavior, showing an initial equilibration phase within the first few picoseconds followed by stable oscillations around 298 K for all adsorption systems.

Extending the simulations to 500 ps (**Table S6**) provides deeper insight into the long-term stability of the Cmt-surface interactions. Across all systems, the average total, potential, and kinetic energies exhibit reduced standard deviations compared to the 100 ps runs, indicating enhanced equilibration and improved statistical reliability at longer simulation times. The potential energies converge smoothly, suggesting that no structural degradation or desorption events occur during the extended simulations. In particular, the doped systems (B@C_3N_4, P@C_3N_4, S@C_3N_4, and Si@C_3N_4) maintain stable energetic profiles, confirming that heteroatom doping does not compromise the thermal or structural integrity of the adsorption complexes.

The temperature evolution at 500 ps, shown in **Figure 5(b)**, demonstrates excellent thermal stability across all systems, with temperature fluctuations tightly centered around 298 K and significantly narrower distributions than during the initial equilibration phase. This behavior validates the suitability of the Nose thermostat and confirms that the MD simulations were well-controlled over extended timescales. Notably, the consistency between the energetic trends in **Tables S5 and S6** and the temperature plots indicates that the systems reached and maintained thermodynamic equilibrium.

View Article Online
DOI: 10.1039/D6MA00432F

The MD results confirm that cimetidine remains stably adsorbed on both pristine and X-doped C_3N_4 surfaces throughout the simulation durations. The close agreement between energy convergence and temperature stabilization across both 100 ps and 500 ps simulations highlights the robustness of the adsorption complexes. It supports their suitability for subsequent analyses, including RDF, MSD, and diffusion coefficient evaluations related to drug transport and release behavior.

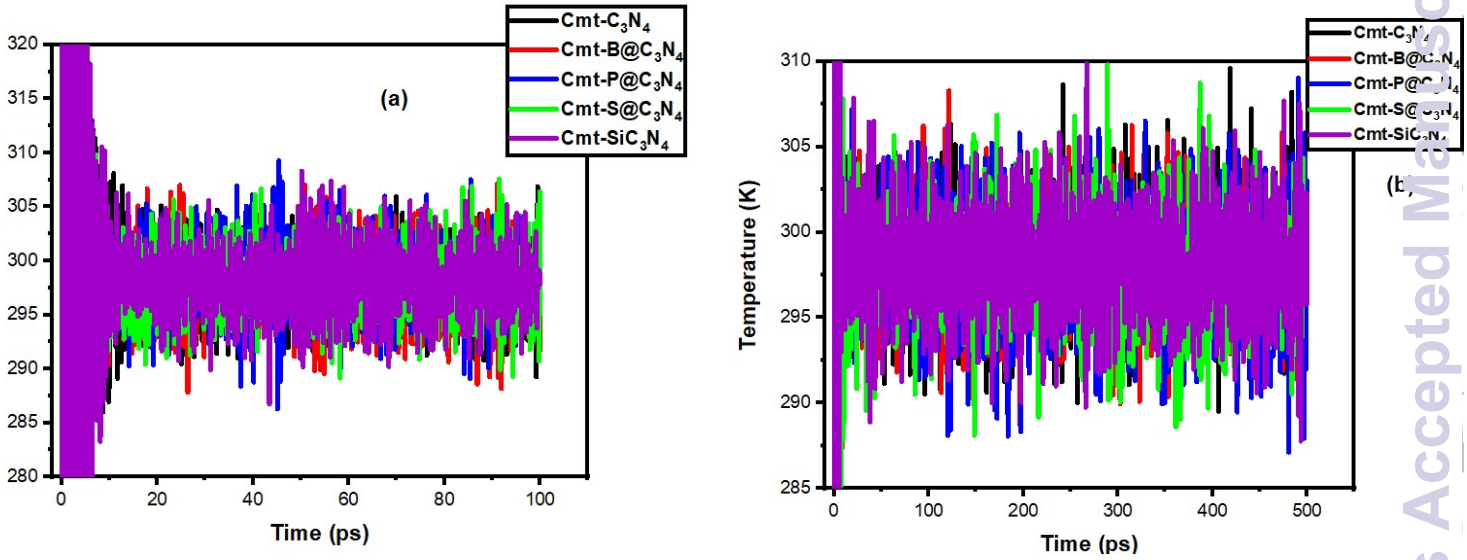

Figure 5. Temperature evolution as a function of simulation time for cimetidine (Cmt) adsorbed on pristine and X-doped C_3N_4 surfaces (X = B, P, S, Si): (a) 100 ps simulation and (b) 500 ps simulation. The plots demonstrate stable thermal equilibration around 298 K, confirming the reliability of the NVT molecular dynamics simulations.

View Article Online
DOI: 10.1039/D6MA00432F

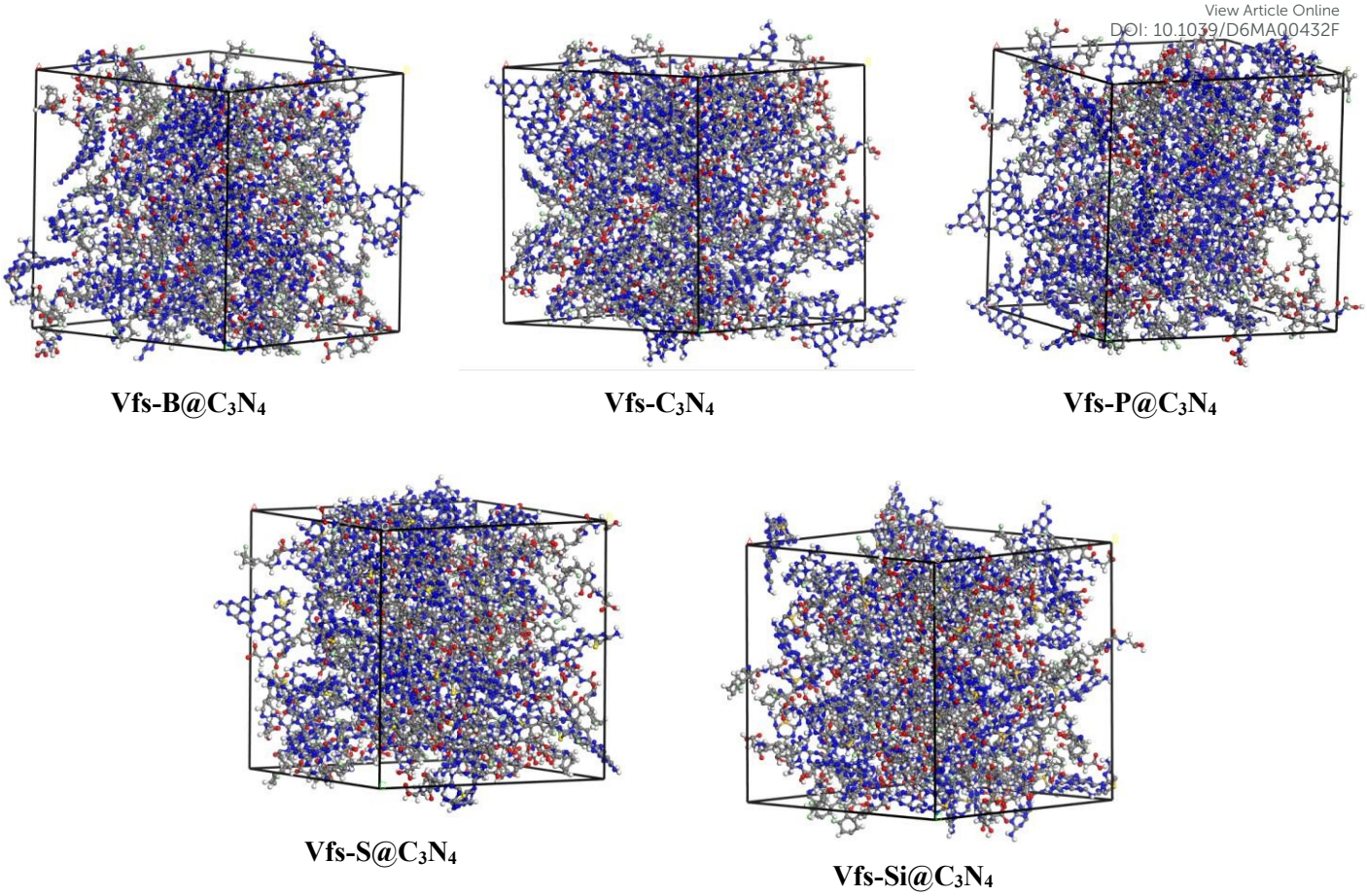

Figure 6. Representative amorphous cell configurations of cimetidine (Cmt) interacting with pristine and X-doped C_3N_4 surfaces (X = B, P, S, Si) were constructed before molecular dynamics simulations. Each periodic simulation box contains 50 C_3N_4-based sheets and 100 cimetidine molecules, corresponding to surface and drug weight fractions of 49.59% and 50.41%, respectively. The disordered packing illustrates the homogeneous dispersion of cimetidine around the doped and undoped C_3N_4 frameworks and provides realistic initial configurations for subsequent NVT molecular dynamics simulations and dynamical analyses.

Biocompatibility and toxicity concerns of doped C_3N_4 systems are important for translating the present computational findings into biomedical applications. In general, graphitic carbon nitride (g-C_3N_4) has been widely reported as a low-toxicity, chemically stable, and potentially biocompatible material, which has enabled its exploration in drug delivery, imaging, and antibacterial systems [50]. In vitro studies further indicate that g-C_3N_4-based materials can exhibit dose-dependent cytotoxicity, often showing good cell viability at low to moderate concentrations, while higher exposure levels may induce reactive oxygen species (ROS)-related stress depending on morphology and surface chemistry [51]. Importantly, doping (B, P, S, Si) may modify surface reactivity and electronic properties, which could influence biological

View Article Online
DOI: 10.1039/D6MA00432F

interactions; however, existing literature generally suggests that properly engineered g-C_3N_4 derivatives remain within acceptable biosafety limits, especially when surface-functionalized or used in controlled delivery systems [52]. Therefore, while doped C_3N_4 systems appear promising for biomedical applications, systematic experimental cytotoxicity and in vivo studies are still required to fully validate long-term safety.

3.6.1 Mean Square Displacement (MSD) and Diffusion Coefficient

The transport behavior of cimetidine (Cmt) within pristine and X-doped C_3N_4 matrices was evaluated using the mean square displacement (MSD) and the corresponding diffusion coefficients extracted from the linear region of the MSD–time profiles. As shown in **Figure 7 (c) and (e)**, the MSD curves for all systems increase monotonically with simulation time at both 100 ps and 500 ps, confirming diffusive motion of cimetidine molecules within the amorphous matrices. At 100 ps, the pristine Cmt-C_3N_4 system exhibits the steepest MSD slope, indicating relatively higher molecular mobility compared to the doped systems. Among the dopants, B@C_3N_4 shows the lowest MSD values over the entire time window, suggesting stronger drug–surface interactions that restrict translational motion. In contrast, P@C_3N_4 and S@C_3N_4 display intermediate MSD behavior, while Si@C_3N_4 shows slightly higher mobility than B- and S-doped systems but remains lower than pristine C_3N_4.

The diffusion coefficients calculated from the MSD data at 100 ps (**Figure 7 (d)**) further support these trends. Cimetidine exhibits the highest diffusion coefficient on pristine C_3N_4, whereas B@C_3N_4 yields the lowest value, reflecting enhanced confinement and stronger adsorption of the drug on boron-doped sites. P@C_3N_4 and S@C_3N_4 show moderate diffusion coefficients, consistent with balanced interactions that allow partial mobility while maintaining adsorption stability. Si@C_3N_4 presents a diffusion coefficient lower than pristine C_3N_4 but higher than B@C_3N_4, indicating comparatively weaker binding than boron doping but stronger than the undoped surface.

At the extended simulation time of 500 ps (**Figure 7 (e) and (f)**), the MSD curves become smoother and more linear, indicating that the systems have reached a well-equilibrated diffusive regime. The diffusion coefficients at 500 ps are uniformly lower than those obtained at 100 ps, which is expected as longer simulations capture sustained drug–surface interactions and reduce the influence of initial ballistic motion. Notably, B@C_3N_4 continues to show the lowest diffusion coefficient, confirming its strong immobilization effect on cimetidine, while pristine C_3N_4 maintains relatively higher diffusivity. The reduced diffusion observed for P-, S-

, and Si-doped systems highlights the role of heteroatom doping in tuning drug mobility through altered surface polarity and interaction strength. The MSD and diffusion coefficient analyses demonstrate that X-doping of C_3N_4 significantly modulates the mobility of cimetidine within the carrier matrix. Stronger interactions, particularly in the B-doped system, lead to reduced diffusion and enhanced drug retention, which is advantageous for controlled and sustained drug delivery. Conversely, higher mobility on pristine C_3N_4 suggests faster drug release, emphasizing the importance of dopant selection in designing graphene-like C_3N_4 carriers with tailored release profiles.

View Article Online
DOI: 10.1039/D6MA00432F

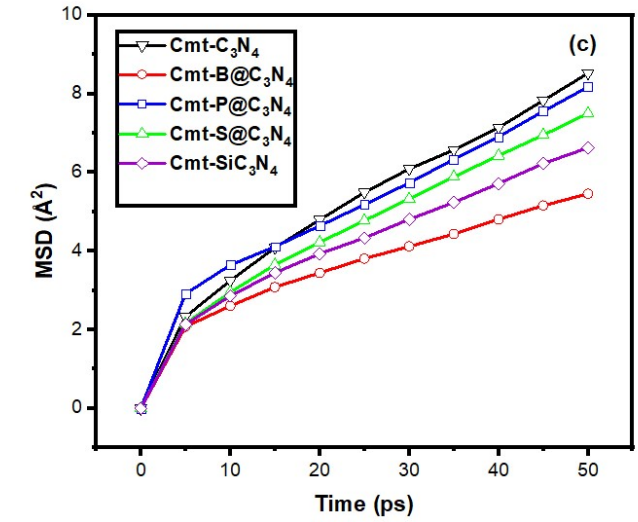

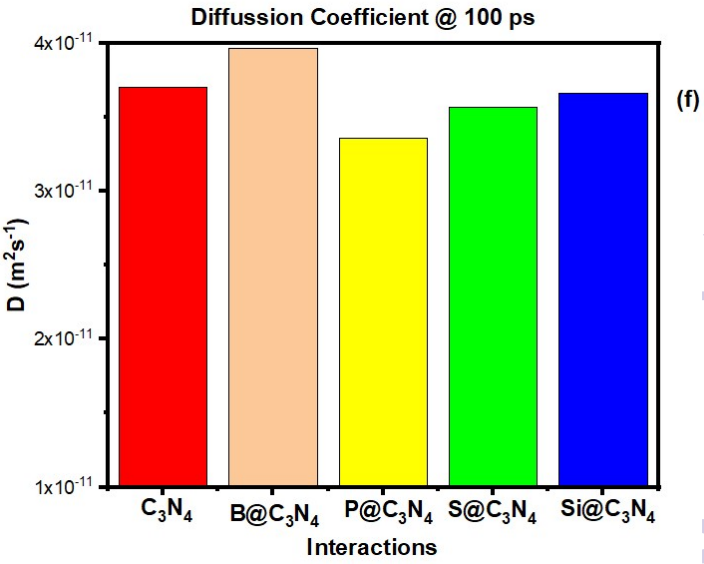

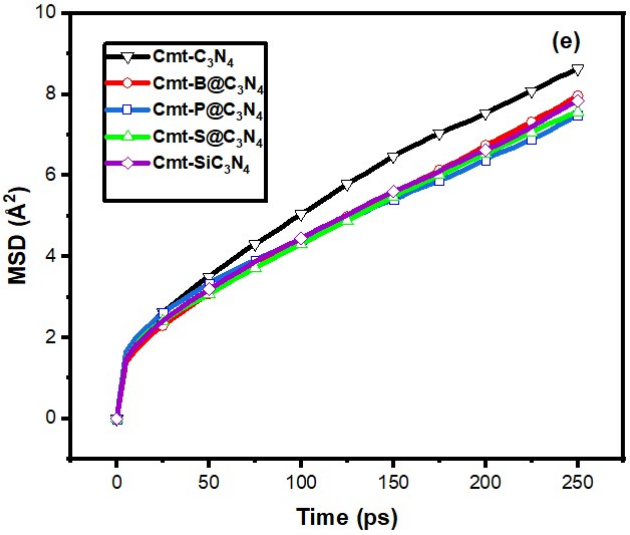

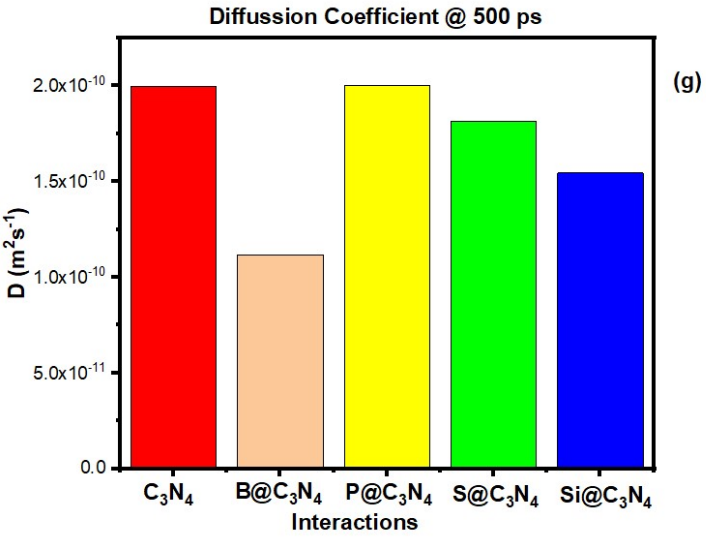

Figure 7. Molecular dynamics analysis of cimetidine (Cmt) mobility on pristine and X-doped C_3N_4 surfaces (X = B, P, S, Si) at 298 K. (c) Mean square displacement (MSD) profiles illustrating the time-dependent translational mobility of cimetidine during NVT simulations at 100 ps. (d) Diffusion coefficients of cimetidine derived from the linear region of the MSD curves using the Einstein relation, highlighting differences in drug mobility and release behavior across the investigated carriers at 100 ps. (e) Extended-time MSD plots demonstrating the long-time diffusive regime relevant to sustained drug release at 500 ps. (f) Diffusion coefficients of cimetidine derived from the linear region of the MSD curves using the Einstein relation, highlighting differences in drug mobility and release behavior across the investigated carriers at 500 ps.

View Article Online
DOI: 10.1039/D6MA00432F

3.6.2 Radial Distribution Function (RDF)

The radial distribution function (RDF), g(r), was employed to further elucidate the microscopic structural organization and interaction strength between cimetidine (Cmt) and the pristine and X-doped C_3N_4 surfaces. **Figure 8 (g) and (h)** present the RDF profiles at 100 ps and 500 ps, respectively, providing insight into both short-range ordering and the temporal evolution of drug–surface interactions. At 100 ps (**Figure 8 (g)**), all systems exhibit pronounced first coordination peaks in the short-range region between approximately 1.0 and 2.0 Å, indicating strong local interactions between cimetidine functional groups and the surface active sites. Among the studied systems, Cmt-Si@C_3N_4 and Cmt-B@C_3N_4 display the highest first peak intensities, suggesting stronger short-range ordering and closer contact distances, which is consistent with enhanced adsorption and reduced molecular mobility observed in the MSD analysis. The pristine Cmt-C_3N_4 system exhibits comparatively lower peak intensities, reflecting weaker intermolecular ordering and more facile diffusion at early simulation times. Secondary peaks around 2.5–3.0 Å correspond to extended interaction shells and indicate the presence of hydrogen bonding and van der Waals interactions contributing to adsorption stabilization. At 500 ps (**Figure 8 (h)**), the RDF profiles become more refined and stabilized across all systems, reflecting equilibration of the drug–carrier complexes. The persistence of sharp first peaks at short distances confirms that the adsorption configurations remain stable over longer timescales. Notably, B@C_3N_4 and P@C_3N_4 systems show sustained high peak intensities, indicating long-lived and well-defined coordination environments for cimetidine, in agreement with their reduced diffusion coefficients at 500 ps. In contrast, the pristine C_3N_4 system continues to exhibit broader and less intense peaks, suggesting weaker confinement and greater spatial freedom for the drug molecule.

At larger radial distances ($r > 4$ Å), g(r) approaches unity for all systems, indicating a transition to bulk-like behavior and the absence of long-range ordering, which is characteristic of amorphous and weakly structured adsorption environments. The bar chart insets further emphasize the comparative peak intensities, highlighting the role of heteroatom doping in enhancing short-range drug–surface interactions. The RDF analysis corroborates the MSD and diffusion coefficient results by confirming that heteroatom doping strengthens local structural ordering and adsorption stability, particularly for B-, P-, and Si-doped C_3N_4. These features are critical for controlled drug retention and sustained release, reinforcing the suitability of doped C_3N_4 frameworks as promising carriers for cimetidine delivery.

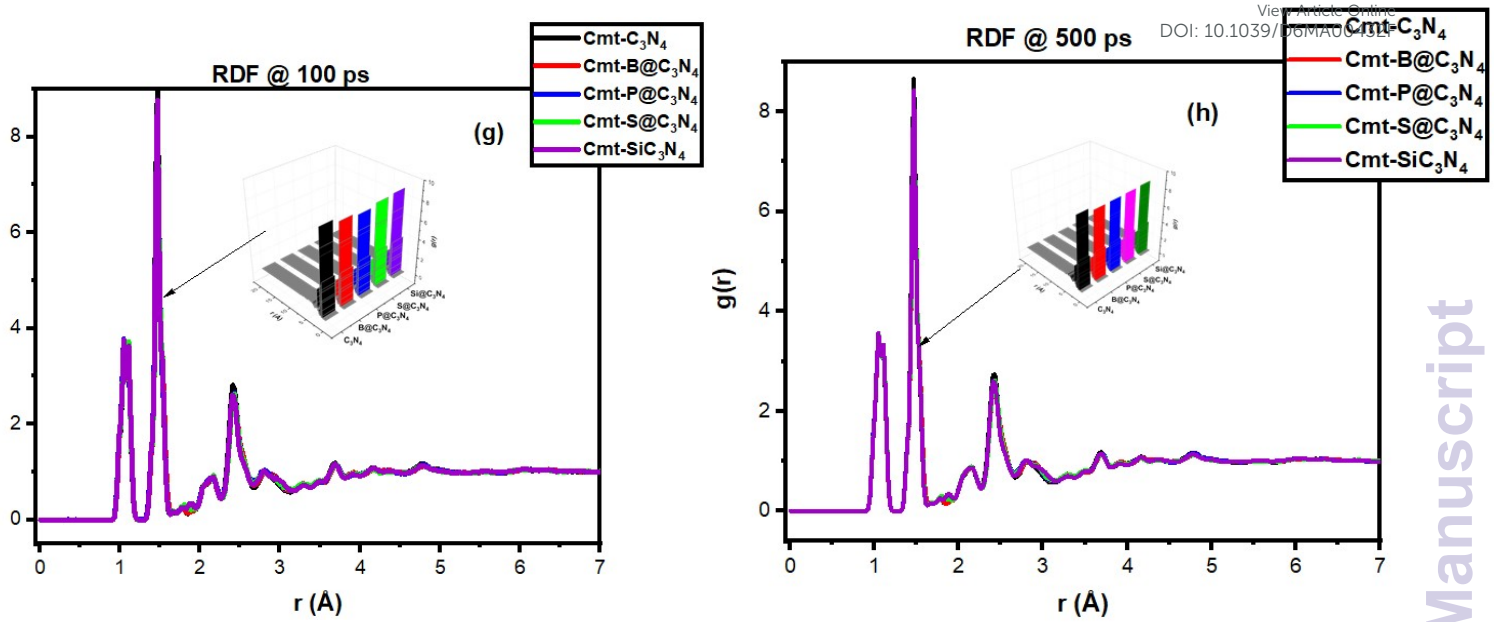

Figure 8. Radial distribution function (RDF) analysis of cimetidine (Cmt) interacting with pristine and X-doped C_3N_4 surfaces. (g) RDF profiles between cimetidine, pristine C_3N_4, and X-doped C_3N_4 surfaces (X = B, P, S, Si), showing preferred intermolecular distances and coordination features indicative of noncovalent drug–surface interactions at 100 ps. (h) RDF profiles between cimetidine, pristine C_3N_4, and X-doped C_3N_4 surfaces (X = B, P, S, Si), showing preferred intermolecular distances and coordination features indicative of noncovalent drug–surface interactions at 500 ps.

4.0 Conclusions

This study presents a systematic computational investigation of pristine and X-doped C_3N_4 (X = B, S, P, and Si) as potential nanocarriers for the cimetidine ulcer drug using DFT and molecular dynamics simulations. Geometry optimization confirmed that heteroatom doping induces significant structural distortions and electronic redistribution within the C_3N_4 framework, creating active adsorption sites for drug binding. Adsorption energy analysis demonstrated that Cmt interacts favorably with all surfaces. Electronic structure analyses, including DOS and NBO, revealed substantial orbital overlap and charge transfer upon adsorption, particularly in doped systems, underscoring the enhanced reactivity imparted by heteroatom substitution. QTAIM and NCI analyses confirmed that adsorption is governed by a synergistic combination of hydrogen bonding, electrostatic interactions, and dispersion forces, with doped systems exhibiting stronger and more directional noncovalent interactions than pristine C_3N_4. Molecular dynamics simulations at physiological temperature verified the thermal stability of all drug–carrier complexes over extended timescales. MSD and diffusion coefficient analyses showed that heteroatom doping effectively modulates cimetidine mobility,

View Article Online
DOI: 10.1039/D6MA00432F

with B-, S-, and Si-doped C_3N_4 achieving an optimal balance between confinement and diffusion. RDF analysis further confirmed stable short-range ordering and persistent drug–surface interactions throughout the simulations. Collectively, these results demonstrate that heteroatom doping is a powerful strategy for tuning the adsorption strength, electronic response, and dynamic behavior of C_3N_4-based drug carriers. Among the investigated systems, B@C_3N_4, S@C_3N_4, and Si@C_3N_4 emerge as the most promising candidates for controlled cimetidine delivery, offering enhanced stability without compromising drug mobility. This work provides valuable molecular-level insight into the design of graphene-derived nanocarriers for gastrointestinal drug delivery applications.

5.0 Declarations

Competing Interest

The authors declare that they have no known competing financial interests or personal relationships that could have appeared to influence the work reported in this paper.

Ethical Approval

Not applicable. This study did not involve human research participants or live vertebrates.

Consent to Participation

Not applicable. This study did not involve human research participants.

Consent to Publish

Not applicable. No participants were involved in this study.

5.1 Funding

This research was not funded by any Governmental or Non-governmental agency.

5.2 Availability of data and material

All data are contained within the manuscript and the manuscript supporting information (SI) documents. Optimized (log) files are available on request.

5.2 Availability of data and material

All data are contained within the manuscript and the manuscript's supporting information (SI) documents. Optimized (log) files are available on request.

View Article Online
DOI: 10.1039/D6MA00432F

5.3 Authors' Contribution

F.A.N: Conceptualization, Supervision, Investigation, Methodology, Writing – original draft, Project administration. **K.E**: Writing – original draft, Data curation, Formal analysis, Investigation; **K.W.Q**: Data curation, Investigation, Writing – original draft; **R.M**: Methodology, Writing – original draft, Writing – review & editing, Validation; : Visualization, Writing – review & editing

5.4 Acknowledgements

We acknowledged the centre for High-Performance Computing Centre, South Africa, for the computational resources.

References

[1] A. Lanas, F. C.-T. Lancet, and undefined 2017, "Peptic ulcer disease," *thelancet.comA Lanas, FKL ChanThe Lancet, 2017•thelancet.com*, vol. 390, 2017, doi: 10.1016/S0140-6736(16)32404-7.

[2] T. Tomita *et al.*, "Successful eradication of Helicobacter pylori prevents relapse of peptic ulcer disease," *Wiley Online LibraryT Tomita, Y Fukuda, K Tamura, J Tanaka, N Hida, T Kosaka, K Hori, T Sakagami, M SatomiAlimentary pharmacology & therapeutics, 2002•Wiley Online Library*, vol. 16, no. 2, pp. 204–209, 2002, doi: 10.1046/J.1365-2036.16.S2.24.X.

[3] J. L. Goldstein, S. C. Lowry, F. L. Lanza, H. I. Schwartz, and W. E. Dodge, "The impact of low-dose aspirin on endoscopic gastric and duodenal ulcer rates in users of a non-selective non-steroidal anti-inflammatory drug or a cyclo," *Wiley Online Library*, vol. 23, no. 10, pp. 1489–1498, May 2006, doi: 10.1111/J.1365-2036.2006.02912.X.

[4] X. Ren *et al.*, "Sulfur-doped graphene-based immunological biosensing platform for multianalysis of cancer biomarkers," *ACS Publications*, vol. 9, no. 43, pp. 37637–37644, Nov. 2017, doi: 10.1021/ACSAMI.7B13416.

[5] M. Li *et al.*, "Tuning sulfur doping in graphene for highly sensitive dopamine biosensors," *Elsevier*, Accessed: Dec. 19, 2025. [Online]. Available: https://www.sciencedirect.com/science/article/pii/S0008622315000469

[6] F. Shahzad, S. Zaidi, C. K.-S. and A. B. Chemical, and undefined 2017, "Highly sensitive electrochemical sensor based on environmentally friendly biomass-derived sulfur-doped graphene for cancer biomarker detection," *Elsevier*, Accessed: Dec. 19, 2025. [Online]. Available: https://www.sciencedirect.com/science/article/pii/S0925400516317798

[7] S. Tan, H. Poh, Z. Sofer, M. P.- Analyst, and undefined 2013, "Boron-doped graphene and boron-doped diamond electrodes: detection of biomarkers and resistance to fouling," *pubs.rsc.org*, Accessed: Dec. 19, 2025. [Online]. Available: https://pubs.rsc.org/en/content/articlehtml/2013/an/c3an00535f

[8] M. P.-J. of M. C. C and undefined 2014, "Heteroatom modified graphenes: electronic and electrochemical applications," *pubs.rsc.org*, Accessed: Dec. 19, 2025. [Online]. Available: https://pubs.rsc.org/en/content/articlehtml/2014/tc/c4tc00336e

[9] P. Lazar, R. Zbořil, M. Pumera, M. O.-C. C. Physics, and undefined 2014, "Chemical nature of boron and nitrogen dopant atoms in graphene strongly influences its electronic properties," *pubs.rsc.org*, Accessed: Dec. 19, 2025. [Online]. Available: https://pubs.rsc.org/en/content/articlehtml/2014/cp/c4cp01638f

[10] M. Ubhi, M. Kaur, J. Grewal, V. S.- Materials, and undefined 2023, "Phosphorous-and boron-doped graphene-based nanomaterials for energy-related applications," *mdpi.com*, Accessed: Dec. 19, 2025. [Online]. Available: https://www.mdpi.com/1996-1944/16/3/1155

[11] R. Mugunthini, B. Anitha, J. Sneha, … R. H.-J. of M., and undefined 2025, "Next-generation Nanocarrier material prescreening: Unlocking silicon-doped graphdiyne through DFT insights," *Elsevier*, Accessed: Dec. 19, 2025. [Online]. Available: https://www.sciencedirect.com/science/article/pii/S109332632500261X

[12] S. Mudedla, K. Balamurugan, … M. K.-P. C., and undefined 2016, "Interaction of nucleobases with silicon doped and defective silicon doped graphene and optical properties," *pubs.rsc.org*, Accessed: Dec. 19, 2025. [Online]. Available: https://pubs.rsc.org/en/content/articlehtml/2015/cp/c5cp06059a

[13] X. Liu *et al.*, "Recent developments of doped gC3N4 photocatalysts for the degradation of organic pollutants," *Taylor & Francis*, vol. 51, no. 8, pp. 751–790, 2021, doi: 10.1080/10643389.2020.1734433.

[14] Q. Du *et al.*, "N-Deficient B-Doped g-C3N4/CdS Heterojunction-Based PEC-FL Biosensor Assisted by CRISPR-Cas12a System for Ultrasensitive Determination of microRNA," *ACS Publications*, vol. 97, no. 7, pp. 4049–4056, Feb. 2025, doi: 10.1021/ACS.ANALCHEM.4C05841.

[15] L. M.- J, B. and Bioprocessing, and undefined 2025, "In vitro and In vivo Bioimaging and Photoelectronic Applications of Graphitic Carbon Nitride (g-C3N4) Composite in Drug Delivery Systems for Cancer Cells," *researchgate.net*, Accessed: Dec. 19, 2025. [Online]. Available: https://www.researchgate.net/profile/Loutfy-Madkour/publication/394275602_Bioimaging_and_Photoelectronic_Applications_of_Graphitic_Carbon_Nitride_g-C3N4_Composite_in_Drug_Delivery_Systems_for_Cancer_Cells_Treatment/links/6890aee486911c11bfed4929/Bioimaging-and-Photoelectronic-Applications-of-Graphitic-Carbon-Nitride-g-C3N4-Composite-in-Drug-Delivery-Systems-for-Cancer-Cells-Treatment.pdf

[16] S. Demirci, S. Suner, O. Neli, A. K.- Nanotechnology, and undefined 2023, "B, P, and S heteroatom doped, bio-and hemo-compatible 2D graphitic-carbon nitride (g-C3N4) with antioxidant, light-induced antibacterial, and bioimaging endeavors," *iopscience.iop.org*, doi: 10.1088/1361-6528/AD0125/META.

[17] L. Zheng, H. Zhang, M. Won, E. Kim, M. Li, and J. S. Kim, "Codoping g-C3N4 with boron and graphene quantum dots: Enhancement of charge transfer for ultrasensitive and selective photoelectrochemical detection of dopamine," *Biosens. Bioelectron.*, vol. 224, Mar. 2023, doi: 10.1016/j.bios.2022.115050.

View Article Online
DOI: 10.1039/D6MA00432F

[18] A. C. Ford, B. Delaney, D. Forman, and P. Moayyedi, "Eradication therapy for peptic ulcer disease in Helicobacter pylori positive patients," *cochranelibrary.com*, no. 4, 2009, doi: 10.1002/14651858.CD003840.PUB4/ABSTRACT.

[19] M. H. Sanad, S. B. Challan, F. A. Marzook, S. M. Abd-Elhaliem, and E. A. Marzook, "Radioiodination and biological evaluation of cimetidine as a new highly selective radiotracer for peptic ulcer disorder detection," *degruyterbrill.comMH Sanad, SB Challan, FA Marzook, SM Abd-Elhaliem, EA MarzookRadiochimica Acta, 2021•degruyterbrill.com*, vol. 109, no. 2, pp. 109–117, Feb. 2021, doi: 10.1515/RACT-2020-0046/HTML.

[20] M. Khajavian, S. Kaviani, I. Piyanzina, D. A. Tayurskii, O. V. Nedopekin, and A. Haseli, "Amide-functionalized g-C3N4 nanosheet for the adsorption of arsenite (As3+): Process optimization, experimental, and density functional theory insight," *Colloids Surf. A Physicochem. Eng. Asp.*, vol. 690, p. 133803, Jun. 2024, doi: 10.1016/J.COLSURFA.2024.133803.

[21] M. Khajavian, S. Kaviani, I. Piyanzina, D. A. Tayurskii, and O. V. Nedopekin, "Zn-decorated S,P,B co-doped C2N nanosheet for ibuprofen adsorption: Experimental and density functional theory calculation," *Colloids Surf. A Physicochem. Eng. Asp.*, vol. 680, p. 132702, Jan. 2024, doi: 10.1016/J.COLSURFA.2023.132702.

[22] S. Kaviani, D. A. Tayurskii, O. V. Nedopekin, I. Piyanzina, and E. Shakerzadeh, "Unveiling potential of thiophene-functionalized C3N3 nanosheet as an anode for Li-ion batteries: A DFT-D3 study," *Inorg. Chem. Commun.*, vol. 165, p. 112491, Jul. 2024, doi: 10.1016/J.INOCHE.2024.112491.

[23] D. Koller, P. Blaha, F. T.-J. of P. C. Matter, and undefined 2013, "Hybrid functionals for solids with an optimized Hartree–Fock mixing parameter," *iopscience.iop.org*, doi: 10.1088/0953-8984/25/43/435503/META.

[24] E. Caldeweyher, C. Bannwarth, S. G.-T. J. of chemical, and undefined 2017, "Extension of the D3 dispersion coefficient model," *pubs.aip.org*, Accessed: Dec. 19, 2025. [Online]. Available: https://pubs.aip.org/aip/jcp/article/147/3/034112/595235

[25] A. Hellweg, D. R.-P. C. C. Physics, and undefined 2015, "Development of new auxiliary basis functions of the Karlsruhe segmented contracted basis sets including diffuse basis functions (def2-SVPD, def2-TZVPPD, and def2," *pubs.rsc.org*, Accessed: Dec. 19, 2025. [Online]. Available: https://pubs.rsc.org/en/content/articlehtml/2014/cp/c4cp04286g

[26] B. Inah, N. Azogor, H. Akpan, … O. L.-C. and, and undefined 2025, "Exploring the adsorption properties of PTFE-decorated and metal doped covalent organic frameworks for environmental cleanup: A computational outlook," *Elsevier*, Accessed: Dec. 19, 2025. [Online]. Available: https://www.sciencedirect.com/science/article/pii/S2210271X25001380

[27] E. D. Glendening, C. R. Landis, and F. Weinhold, "NBO 7.0: New vistas in localized and delocalized chemical bonding theory," *Wiley Online Library*, vol. 40, no. 25, pp. 2234–2241, 2019, doi: 10.1002/JCC.25873.

[28] A. F.- Wallingford, undefined Usa, undefined 25p, and undefined 2009, "gaussian 09W Reference," *orgchem.kpi.ua*, Accessed: Dec. 19, 2025. [Online]. Available: https://orgchem.kpi.ua/files/Gaussian_09_ReferenceManual.pdf

[29] M. García-Valverde, … N. C.-E., and undefined 2015, "GAUSSVIEW® as a tool for learning organic chemistry," *library.iated.org*, Accessed: Dec. 19, 2025. [Online]. Available: https://library.iated.org/view/GARCIAVALVERDE2015GAU

[30] W. Humphrey, A. Dalke, K. S.-J. of molecular graphics, and undefined 1996, "VMD: visual molecular dynamics," *Elsevier*, Accessed: Dec. 19, 2025. [Online]. Available: https://www.sciencedirect.com/science/article/pii/0263785596000185

[31] T. Lu, F. C.-J. of computational chemistry, and undefined 2012, "Multiwfn: A multifunctional wavefunction analyzer," *Wiley Online Library*, vol. 33, no. 5, pp. 580–592, Feb. 2012, doi: 10.1002/JCC.22885.

[32] M. Meunier and S. Robertson, "Materials Studio 20th anniversary," *Taylor & Francis*, vol. 47, no. 7, pp. 537–539, 2021, doi: 10.1080/08927022.2021.1892093.

[33] A. K. Rappé, C. J. Casewit, K. S. Colwell, W. A. Goddard, and W. M. Skiff, "UFF, a full periodic table force field for molecular mechanics and molecular dynamics simulations," *ACS Publications*, vol. 114, no. 25, pp. 10024–10035, Dec. 1992, doi: 10.1021/JA00051A040.

[34] X. Liu, Z. R.-J. of the E. Institute, and undefined 2019, "Thermal diffusion and phase transition of n-octadecane as thermal energy storage material on nanoscale copper surface: a molecular dynamics study," *Elsevier*, Accessed: Dec. 19, 2025. [Online]. Available: https://www.sciencedirect.com/science/article/pii/S1743967117304993

[35] P. Yuan, P. Zhang, T. Liang, S. Zhai, and D. Yang, "Effects of functionalization on energy storage properties and thermal conductivity of graphene/n-octadecane composite phase change materials," *SpringerP Yuan, P Zhang, T Liang, S Zhai, D YangJournal of Materials Science, 2019•Springer*, vol. 54, no. 2, pp. 1488–1501, Jan. 2019, doi: 10.1007/S10853-018-2883-2.

[36] K. Asif, M. Perveen, R. Khera, S. Nazir, … A. A.-C. and, and undefined 2021, "Computational and theoretical study of graphitic carbon nitride (g-C3N4) as a drug delivery carrier for lonidamine drug to treat cancer," *Elsevier*, Accessed: Dec. 20, 2025. [Online]. Available: https://www.sciencedirect.com/science/article/pii/S2210271X21003170

[37] D. Zhu, Q. Z.-A. C. B. Environmental, and undefined 2021, "Nitrogen doped g-C3N4 with the extremely narrow band gap for excellent photocatalytic activities under visible light," *Elsevier*, Accessed: Dec. 20, 2025. [Online]. Available: https://www.sciencedirect.com/science/article/pii/S0926337320308894

[38] A. Klein *et al.*, "The Fermi energy as common parameter to describe charge compensation mechanisms: A path to Fermi level engineering of oxide electroceramics," *J. Electroceram.*, vol. 51, no. 3, pp. 147–177, Nov. 2023, doi: 10.1007/S10832-023-00324-Y.

[39] M. Lamanec, "From Theory to Experiment: A Computational Chemistry Perspective on Dative Bond and Non-Covalent Interactions," *theses.cz*, Accessed: Dec. 20, 2025. [Online]. Available: https://theses.cz/id/fvudbo/Lamanec_PhD_thesis_Archive.pdf

[40] B. Huwaimel, S. A.-S. Reports, and undefined 2025, "A DFT investigation of the adsorption mechanism of paclitaxel on functionalized graphene oxide for enhanced drug delivery," *nature.com*, Accessed: Dec. 20, 2025. [Online]. Available: https://www.nature.com/articles/s41598-025-99156-9

[41] F. Safdari, H. Raissi, M. Shahabi, and M. Zaboli, "DFT Calculations and Molecular Dynamics Simulation Study on the Adsorption of 5-Fluorouracil Anticancer Drug on Graphene Oxide Nanosheet as a Drug Delivery Vehicle," *Journal of Inorganic and Organometallic Polymers and Materials 2017 27:3*, vol. 27, no. 3, pp. 805–817, Mar. 2017, doi: 10.1007/S10904-017-0525-9.

[42] O. Leenaerts, B. Partoens, and F. M. Peeters, "Adsorption of H2O, NH3, CO, NO2, and NO on graphene: A first-principles study," *Phys. Rev. B Condens. Matter Mater. Phys.*, vol. 77, no. 12, Oct. 2007, doi: 10.1103/PhysRevB.77.125416.

[43] D. K. Miller, C. Loy, and S. V. Rosokha, "Examining a transition from supramolecular halogen bonding to covalent bonds: topological analysis of electron densities and energies in the complexes of," *ACS Publications*, vol. 6, no. 36, pp. 23588–23597, Sep. 2021, doi: 10.1021/ACSOMEGA.1C03779.

[44] M. A. Raimi, C. R. Nwokoye, S. S. Effiong, E. K. Aidoo, J. A. Agwupuye, and M. Runde, "Exploring Group 13 (B, Al, Ga, In) mono-doped fullerenes ($C_{59}X$) for methane adsorption: a DFT and QTAIM investigation," *Springer*, vol. 27, no. 8, Aug. 2025, doi: 10.1007/S11051-025-06396-X.

[45] C. Lefebvre, G. Rubez, … H. K.-P. C., and undefined 2017, "Accurately extracting the signature of intermolecular interactions present in the NCI plot of the reduced density gradient versus electron density," *pubs.rsc.org*, Accessed: Dec. 20, 2025. [Online]. Available: https://pubs.rsc.org/en/content/articlehtml/2005/zq/c7cp02110k

[46] U. Orozco-Valencia, J. L. Gázquez, and A. Vela, "Donation and back-donation analyzed through a charge transfer model based on density functional theory," *Springer*, vol. 23, no. 7, Jul. 2017, doi: 10.1007/S00894-017-3368-Y.

[47] L. Lin, R. Jacobs, T. Ma, D. Chen, J. Booske, and D. Morgan, "Work function: Fundamentals, measurement, calculation, engineering, and applications," *APS*, vol. 19, no. 3, Mar. 2023, doi: 10.1103/PHYSREVAPPLIED.19.037001.

[48] N. M.-J. of P. C. Matter and undefined 2017, "Charge transfer in time-dependent density functional theory," *iopscience.iop.org*, doi: 10.1088/1361-648X/AA836E/META.

[49] D. Hait, M. H.-G.-J. of chemical theory and, and undefined 2018, "How accurate is density functional theory at predicting dipole moments? An assessment using a new database of 200 benchmark values," *ACS Publications*, vol. 14, no. 4, pp. 1969–1981, Apr. 2018, doi: 10.1021/ACS.JCTC.7B01252.

[50] G. Liao *et al.*, "Emerging graphitic carbon nitride-based materials for biomedical applications," *Prog. Mater. Sci.*, vol. 112, p. 100666, Jul. 2020, doi: 10.1016/J.PMATSCI.2020.100666.

[51] Z. Durmus, F. Ozdemir, Z. O. Çalışkaner, A. W. Maijenburg, A. Durmus, and R. Köferstein, "Effect of the structural features of graphitic carbon nitride (g-C3N4) synthesized via thermal polycondensation of different precursors on the in vitro tumor cell cytotoxicity," *Diam. Relat. Mater.*, vol. 160, p. 113064, Dec. 2025, doi: 10.1016/J.DIAMOND.2025.113064.

[52] R. Jia *et al.*, "Recent advances in graphitic carbon nitride-based heterojunction for biomedical applications," *Chemical Engineering Journal*, vol. 500, p. 157464, Nov. 2024, doi: 10.1016/J.CEJ.2024.157464.